Kaunas University of Technology

Faculty of Mathematics and Natural Sciences

EEG Signal Analysis for Alzheimer's Disease and Frontotemporal Dementia Recognition Using Statistical and Deep Learning Methods

Master's Final Degree Project

Vesta Kubiliūtė

Project author

Assoc. Prof. Dr. Karolina Armonaitė

Supervisor

Kaunas, 2026

Kaunas University of Technology

Faculty of Mathematics and Natural Sciences

EEG Signal Analysis for Alzheimer's Disease and Frontotemporal Dementia Recognition Using Statistical and Deep Learning Methods

Master's Final Degree Project

Data Science and Artificial Intelligence (6211AX013)

Vesta Kubiliūtė

Project author

Assoc. Prof. Dr. Karolina Armonaitė

Supervisor

Assoc. Prof. Dr. Tomas Iešmantas

Reviewer

Kaunas, 2026

Kaunas University of Technology

Faculty of Mathematics and Natural Sciences

Vesta Kubiliūtė

EEG Signal Analysis for Alzheimer's Disease and Frontotemporal Dementia Recognition Using Statistical and Deep Learning Methods

Declaration of Academic Integrity

I confirm the following:

1. I have prepared the final degree project independently and honestly without any violations of the copyrights or other rights of others, following the provisions of the Law on Copyrights and Related Rights of the Republic of Lithuania, the Regulations on the Management and Transfer of Intellectual Property of Kaunas University of Technology (hereinafter – University) and the ethical requirements stipulated by the Code of Academic Ethics of the University;

2. All the data and research results provided in the final degree project are correct and obtained legally; none of the parts of this project are plagiarised from any printed or electronic sources; all the quotations and references provided in the text of the final degree project are indicated in the list of references;

3. I have not paid anyone any monetary funds for the final degree project or the parts thereof unless required by the law;

4. I understand that in the case of any discovery of the fact of dishonesty or violation of any rights of others, the academic penalties will be imposed on me under the procedure applied at the University; I will be expelled from the University and my final degree project can be submitted to the Office of the Ombudsperson for Academic Ethics and Procedures in the examination of a possible violation of academic ethics.

Vesta Kubiliūtė

Confirmed electronically

Kubiliūtė Vesta. EEG Signal Analysis for Alzheimer's Disease and Frontotemporal Dementia Recognition Using Statistical and Deep Learning Methods. Master's Final Degree Project / supervisor Assoc. Prof. Dr. Karolina Armonaitė; Faculty of Mathematics and Natural Sciences, Kaunas University of Technology.

Study field and area (study field group): Mathematical sciences, Applied mathematics.

Keywords: Alzheimer's disease, frontotemporal dementia, EEG, spectral analysis, functional connectivity, machine learning.

Kaunas, 2026. p. 48.

Summary

Alzheimer's disease (AD) is the most common form of dementia, associated with gradual decline in cognitive functions, particularly memory and learning. Another common cause of dementia is frontotemporal dementia (FTD), which is characterised by behavioural changes or language impairments. While there are several diagnostic methods for differentiating dementia subtypes, they are expensive, slow and not widely accessible. Therefore, there is a need for more affordable and accessible differential diagnostic tools. The aim of this study was to implement an EEG signal analysis to recognise AD from FTD using statistical and deep learning methods. Resting-state, closed-eyes electroencephalogram (EEG) recordings from individuals diagnosed with AD and FTD were analysed. Spectral analysis was performed using Fast Fourier Transform, and functional connectivity (FC) was calculated using Pearson's correlation and coherence. The FC matrices were used as input features for a convolutional neural network (CNN) and, for comparison, for a support vector machine (SVM) classifier. The performance of models was evaluated using leave-one-subject-out cross-validation. Feature importance for the CNN classification was obtained using gradient input saliency. The results revealed that theta band power was significantly higher in the AD group compared with the FTD group, while no significant differences were observed in other frequency bands. Furthermore, the AD exhibited a tendency toward higher theta band FC in frontal and posterior temporal regions, while FTD exhibited a tendency toward higher alpha band connectivity in central regions. The CNN-based model achieved higher classification accuracy than the SVM classifier, with accuracies of 85.6% (SD = 25.8) and 57.1% (SD = 35.4). Frontal and occipital region connections were identified as the most important connectivity features for distinguishing between AD and FTD. These results show the potential of EEG features combined with deep learning models as a more affordable and accessible tool for differentiating dementia subtypes.

Kubiliūtė Vesta. EEG signalų analizė Alzheimerio ligos ir frontotemporalinės demencijos atpažinimui, naudojant statistinius ir giliojo mokymosi metodus. Magistro baigiamasis projektas / vadovė Assoc. Prof. Dr. Karolina Armonaitė; Kauno technologijos universitetas, Matematikos ir gamtos mokslų fakultetas.

Studijų kryptis ir sritis (studijų krypčių grupė): Matematikos mokslai, Taikomoji matematika.

Reikšminiai žodžiai: Alzheimerio liga, frontotemporalinė demencija, EEG, spektrinė analizė, funkcinis ryšys, mašininis mokymasis.

Kaunas, 2026. 48 p.

Santrauka

Alzheimerio liga (AD) – tai dažniausia demencijos forma, susijusi su progresuojančiu kognityvinių funkcijų silpnėjimu, ypač atminties ir mokymosi. Kita dažna demencijos forma – frontotemporalinė demencija (FTD), kuriai būdingi elgesio pokyčiai arba kalbos sutrikimai. Nors egzistuoja keletas diagnostikos metodų, leidžiančių atskirti demencijos formas, tačiau jie yra brangūs, lėti ir ne visiems prieinami. Todėl reikalingos pigesnės ir labiau prieinamos diferencinės diagnostikos priemonės. Šio tyrimo tikslas – atlikti EEG signalų analizę, taikant statistinius ir gilumino mokymosi metodus, siekiant atskirti AD nuo FTD. Tyrime analizuoti ramybės būsenos, užmerktų akių elektroencefalogramos (EEG) įrašai iš asmenų, kuriems diagnozuota AD ir FTD. Spektrinė analizė buvo atlikta naudojant greitą Furjė transformaciją, o funkcinis ryšys (FC) apskaičiuotas taikant Pearsono koreliaciją ir koherenciją. FC matricos buvo naudots kaip įvesties požymiai konvoliuciniam neuroniniam tinklui (CNN) ir, palyginimui, atraminio vektoriaus mašinos (SVM) klasifikatoriui. Modelių veikimas buvo vertintas naudojant „palik vieną subjektą“ kryžminį validavimą. Požymių svarba CNN klasifikacijai nustatyta naudojant gradientinį įvesties svarbumą. Rezultatai parodė, kad AD grupės teta bangų galia buvo reikšmingai didesnė palyginti su FTD grupe, o kitose dažnių juostose reikšmingų skirtumų nenustatyta. Be to, pastebėta tendencija, kad AD grupės teta bangų FC didesnis priekinėse ir užpakalinėse smegenų srityse, o FTD grupė pasižymi didesniu alfa bangų ryšiu centrinėse srityse. CNN modelis pasiekė didesnį klasifikavimo tikslumą nei SVM klasifikatorius – atitinkamai 85,6% (SD = 25,8) ir 57,1% (SD = 35,4). Priekinės ir pakaušinės sričių jungtys buvo nustatytos kaip svarbiausios savybės, leidžiančios atskirti AD ir FTD. Šie rezultatai rodo EEG savybės, derinamos su giliojo mokymosi modeliais, turi potencialą tapti pigesne ir lengviau pasiekiama priemone demencijos tipams diferencijuoti.

Table of contents

List of figures

List of tables

List of abbreviations

AD – Alzheimer's disease

FTD – frontotemporal dementia

EEG – electroencephalography

HC – healthy controls

MND – major neurocognitive disorder

LBD – Lewy body dementia

Aβ – beta-amyloid

NFTs – neurofibrillary tangles

MMSE – Mini-Mental State Examination

MoCA – Montreal Cognitive Assessment

MRI – magnetic resonance imaging

CT – computed tomography

PET – positron emission tomography

SPECT – single photon emission computed tomography

fMRI – functional magnetic resonance imaging

CSF – cerebrospinal fluid

Aβ42 – beta-amyloid of 42 amino acids

t-tau – total tau

p-tau – phosphorylated tau

NfL – neuroflaminent light chain

bvFTD – behavioural variant frontotemporal dementia

nfvPPA – non-fluent/agrammatic variant of primary progressive aphasia

svPPA – semantic variant of primary progressive aphasia

FTLD – frontotemporal lobar degeneration

TDP-43 – transactive response DNA-binding protein 43 kD

FUS – fused in sarcoma protein

BBRC – Brief Cognitive Screening Battery

FDG – fluorodeoxyglucose

PSD – power spectral density

FFT – Fast Fourier Transform

FC – functional connectivity

PLI – phase lag index

ML – machine learning

CNN – convolutional neural network

LNSO – leave-N-subject-out

LOSO – leave-one-subject-out

TF-FC – time-frequency functional connectivity

BF-FC – band-pass filtered functional connectivity

LOO – leave-one-out

ASR – Artifact Subspace Reconstruction

ICA – Independent Component Analysis

DFT – Discrete Fourier Transform

SVM – support vector machine

RBF – radial basis function

Introduction

Dementia is a group of symptoms mainly affecting cognitive functions and social behaviour. Common causes of dementia are Alzheimer's disease (AD), cerebrovascular disease, frontotemporal dementia (FTD) and others [1]. Each dementia subtype is associated with its own characteristic symptoms, but in practice, those symptoms often overlap. For this reason, it becomes more difficult to differentiate between dementia subtypes, during the diagnostic process [2]. Several existing methods, such as cerebrospinal fluid biomarkers, can distinguish types of dementia, but these methods are expensive and not widely accessible in clinical practice. However, each disorder has different treatment strategies, which shows the importance of accurate differentiation [3]. Therefore, there is a need for more accessible and affordable diagnostic tool, which could reliably distinguish between dementia subtypes.

Electroencephalography (EEG) is an affordable and accessible technique that is being intensively investigated by researchers for its potential as a clinical tool for diagnosing various diseases. Moreover, many studies have reported high classification accuracy of classifying individuals with AD and/or FTD from healthy controls (HC), using various EEG features. These previous results show that EEG features can help to identify diseases, and therefore they may be beneficial for differentiating between dementia subtypes. This project analysed EEG recordings obtained from individuals with AD and FTD. The analysis of the recordings was performed to identify EEG features that differ between the two groups and to evaluate the effectiveness of classification using these features.

The aim is to implement an EEG signal analysis to recognise Alzheimer's disease from frontotemporal dementia using statistical and deep learning methods.

Tasks:

1. To analyse spectral characteristics of EEG recordings obtained from individuals diagnosed with Alzheimer's disease and frontotemporal dementia.
2. To examine EEG functional connectivity features in individuals with Alzheimer's disease and frontotemporal dementia.
3. To identify the optimal CNN architecture for the classification of Alzheimer's disease and frontotemporal dementia, using functional connectivity features.
4. To evaluate classification performance across different EEG feature sets and machine learning models.
5. To determine the most important EEG connectivity features for the classification of Alzheimer's disease and frontotemporal dementia.

1. Literature analysis

1.1. Dementia and its major subtypes: Alzheimer's disease and frontotemporal dementia

Significant decline in cognitive abilities that affects an individual's daily functioning and activities is associated with dementia, which is also known as major neurocognitive disorder (MND) [4]. Common causes of dementia include AD, cerebrovascular disease, Lewy body dementia (LBD), FTD and others [5]. More than 50 million people around the world were living with dementia in 2020. The number is expected to triple over the next 25 years, with nearly two-thirds living in low-income and middle-income countries. More specifically, it is predicted that over the next 25 years, cases of dementia will double in Europe [6, 7].

1.1.1. Alzheimer's disease: pathology, treatment and diagnosis

The most common form of dementia is AD, accounting for approximately 60–80% of all dementia cases [8]. Progressive decline in cognitive functions, such as memory and learning, is the main symptoms of AD. The risk of developing AD increases significantly with age. Only 1–6% of all cases are diagnosed before the age of 65, with most people being diagnosed after this age [9]. The development of AD is categorised into four overlapping phases [10]:

- The preclinical or presymptomatic stage: early pathological changes in the cortex and hippocampus begin to occur, which can cause mild memory problems. A person can live in this stage for several years without noticing any symptoms or experiencing any impairment in daily functioning.
- The mild or early stage: symptoms begin to appear and affect everyday life. The most common symptoms are memory loss, distraction, disorientation, and signs of depression.
- The moderate stage: the condition spreads further in the cerebral cortex, which leads to more severe memory loss, difficulty in recognising relatives, and challenges with speaking, writing or reading.
- The severe or late stage: widespread degeneration throughout the entire cortex is observed. Patients living in this stage, experience severe cognitive and functional decline, also may suffer from swallowing and urination difficulties. Eventually, such complications can cause death.

The development of AD is the result of structural and functional deterioration of the brain. This includes synaptic loss, abnormal accumulation of proteins, metabolic impairment and progressive neurodegeneration. Figure 1 illustrates the most important pathological changes associated with AD. One of the primary pathological changes in AD is the formation of amyloid plaques outside the cells, which are composed of beta-amyloid (Aβ) peptides. These Aβ deposits begin to form in the neocortex, subsequently spreading to the hippocampus, subcortical nuclei, and eventually, to the cerebellum [11, 12]. Another important pathological change in AD occurs inside the neurons, where hyperphosphorylated tau proteins accumulate and aggregate to form neurofibrillary tangles (NFTs) [12]. It has been established that the formation of NFTs begins in the internal part of the temporal lobe, gradually progressing to the external part of the temporal lobe and eventually spreads to the posterior cortical association areas and the entire cortex [13]. These amyloid plaques and NFTs are considered to be the main pathological processes that contribute to futher changes in the brain, such as loss of neurons and synapses.

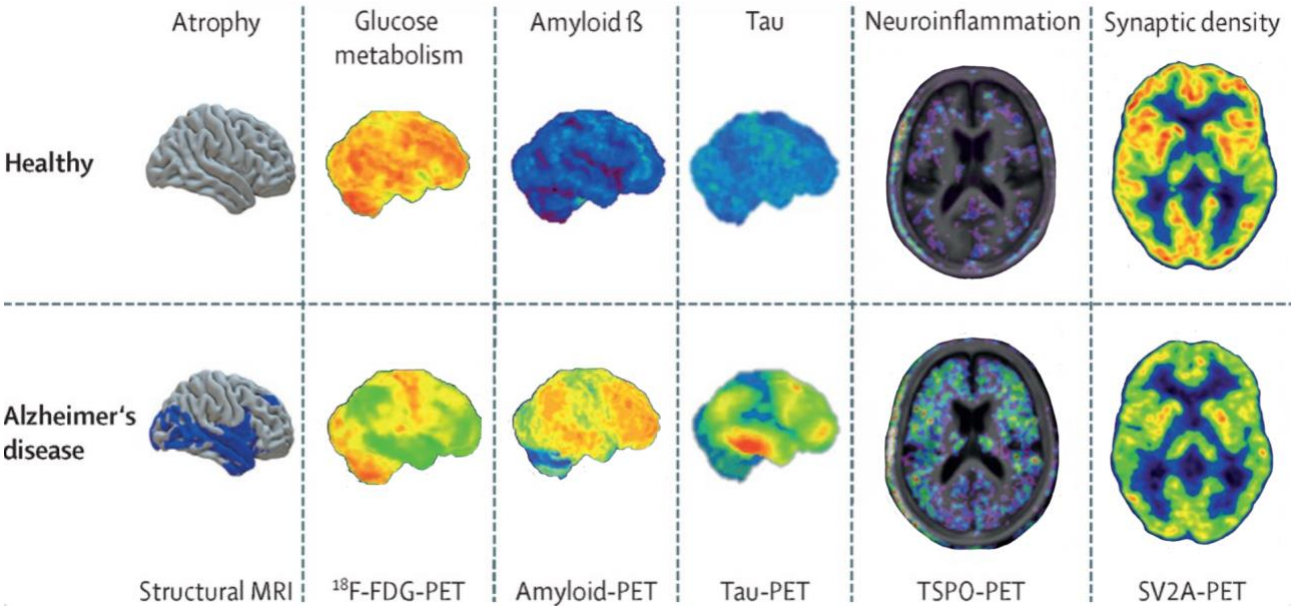

Fig. 1. Comparison of Structural and Molecular Imaging Biomarkers in Healthy Individuals and Alzheimer's Disease Patients [14]

The accumulation of Aβ is connected to the formation of oligomers, which are known to be harmful to the nervous system [8]. These oligomers interact with neuronal membranes directly or by binding to receptors located on the cell surface, which can disrupt signaling inside the neuron, reduce neural activity, stimulate microglia to release harmful mediators. All changes induced by Aβ oligomers eventually affect synaptic plasticity, cause synapse loss, tau pathology, increase oxidative stress, cholinergic dysfunction and neurodegeneration [15, 16]. Furthermore, the vascular system, which is essential for normal brain function, becomes disrupted. As a result, brain recieves insufficient oxygen and nutrients, and is unable to remove metabolic products. Also, dysfunction of the vascular system activates microglia and astrocytes, causing chronic inflammation [17].

Although it is known that NFTs contribute to the pathology of AD, their effects on the neuropil – the dense network of dendrites, axons, and glial processes – are not yet clearly understood. NFTs consist of aggregated hyperphosphorylated tau proteins. In healthy individuals, tau proteins help to maintain the stability and organisation of neuronal microtubules, supporting processes such as intracellular transport. These proteins are strictly regulated and phosphorylated in a controlled manner so that they could bind to microtubules and perform their functions [8, 18]. In the case of AD, tau proteins become abnormally hyperphosphorylated and lose their ability to stabilise microtubules. Such dysfunctional protein detaches from the microtubules and begins to accumulate and aggregate into NFTs. Without tau protein, microtubules lose their stability, which disrupts intracellular transport, neurons become dysfunctional and eventually die, leading to impaired brain function [19]. Moreover, synaptic loss is being observed in the early stages of AD. The contribution of Aβ and tau pathologies disrupts synaptic structure and function, leading to dendritic spine loss, impaired neurotransmission, and eventually synapse elimination. Subsequently, synaptic loss is more accelerated by neuroinflammation caused by activated microglia and astrocytes [20].

Additionally, glucose metabolism impairments are observed in the brains of individuals with AD. The expression of key glucose transporters, such as GLUT1 in the blood–brain barrier and GLUT3

in neurons is reduced. This limits the glucose absorption into the brain, contributing to cerebral hypometabolism, particularly in the cortex and hippocampus. Consequently, ATP production can be reduced by up to 50%, resulting in significant energy deficits as glucose is the primary energy source for neurons. Synaptic communication and plasticity disturbances, increased tau hyperphosphorylation, and impaired normal cell function occur in neurons that do not have enough energy [21–23]. Eventually, all these pathological processes contribute to neuronal death and impaired neuronal communication, which causes memory loss and other cognitive deficits characteristic in AD.

Even though AD has been extensively researched and numerous studies have been conducted over the years, no cure for the disease has yet been found. Current pharmacological treatments can help only with symptom management, but there is no treatment that can cure AD. Currently, there are four approved drugs designed to slow the progression of the disease, temporarily stabilise or enhance cognitive functions, and manage behavioural changes. However, these medications are beneficial only minimally and temporally, as they target the symptoms rather than the underlying cause of the disorder [17]. Additionally, several non-pharmacological therapies can be used to help improve the quality of life for people with AD. Cognitive-based treatments such as cognitive rehabilitation, cognitive training, and cognitive stimulation therapy are the most commonly used therapies, which have demonstrated mild but meaningful benefits, particularly when combined with pharmacological treatment. Individuals diagnosed with AD are also advised to focus on lifestyle changes, such as regulating sleep quality, physical activity, and diet, which may slightly improve cognitive performance and behavioural symptoms [9]. However, both pharmacological and non-pharmacological treatments are most effective when used in the early or presymptomatic stages, before significant neurodegeneration has occurred [17]. This shows how important early diagnosis and timely interventions are in order to make treatment as effective as possible.

During the diagnostic process for AD, clinical evaluations, cognitive testing, advanced neuroimaging methods and biomarkers should be used to ensure reliable diagnosis (Figure 2). When a person is suspected of having AD, the diagnostic process begins with physical examination, standard blood tests, and an analysis of medical and family history. If those findings suggest of a potential cognitive impairments, more detailed assessment of cognitive function is performed using standardised tests. The most common cognitive tests are the Mini-Mental State Examination (MMSE), the Montreal Cognitive Assessment (MoCA). Also, additional functional or behavioural assessments may be employed when necessary [24]. Further evaluation includes neuroimaging, which can reveal structural, functional, and molecular changes in the brain. Magnetic resonance imaging (MRI) and computed tomography (CT) are used to identify brain atrophy, while positron emission tomography (PET), single photon emission computed tomography (SPECT), and functional MRI (fMRI) provide valuable information about metabolism, blood flow, neuroinflammation and the presence of Aβ or tau pathology [8]. Additionally, specific biomarkers can be used to detect metabolites associated with AD. Specific AD biomarkers are categorised into biomarkers obtained from cerebrospinal fluid (CSF), such as Aβ of 42 amino acids (Aβ42), phosphorylated tau (p-tau), and total tau (t-tau), and biomerkers derived from blood, which include Aβ42/40 ratio, p-tau, neuroflaminent light chain (NfL) [8, 25]. The use of these biomarkers and imaging techniques allows the detection of Aβ and tau pathology, along with signs of neurodegeneration, which are important aspects for the AD diagnosis.

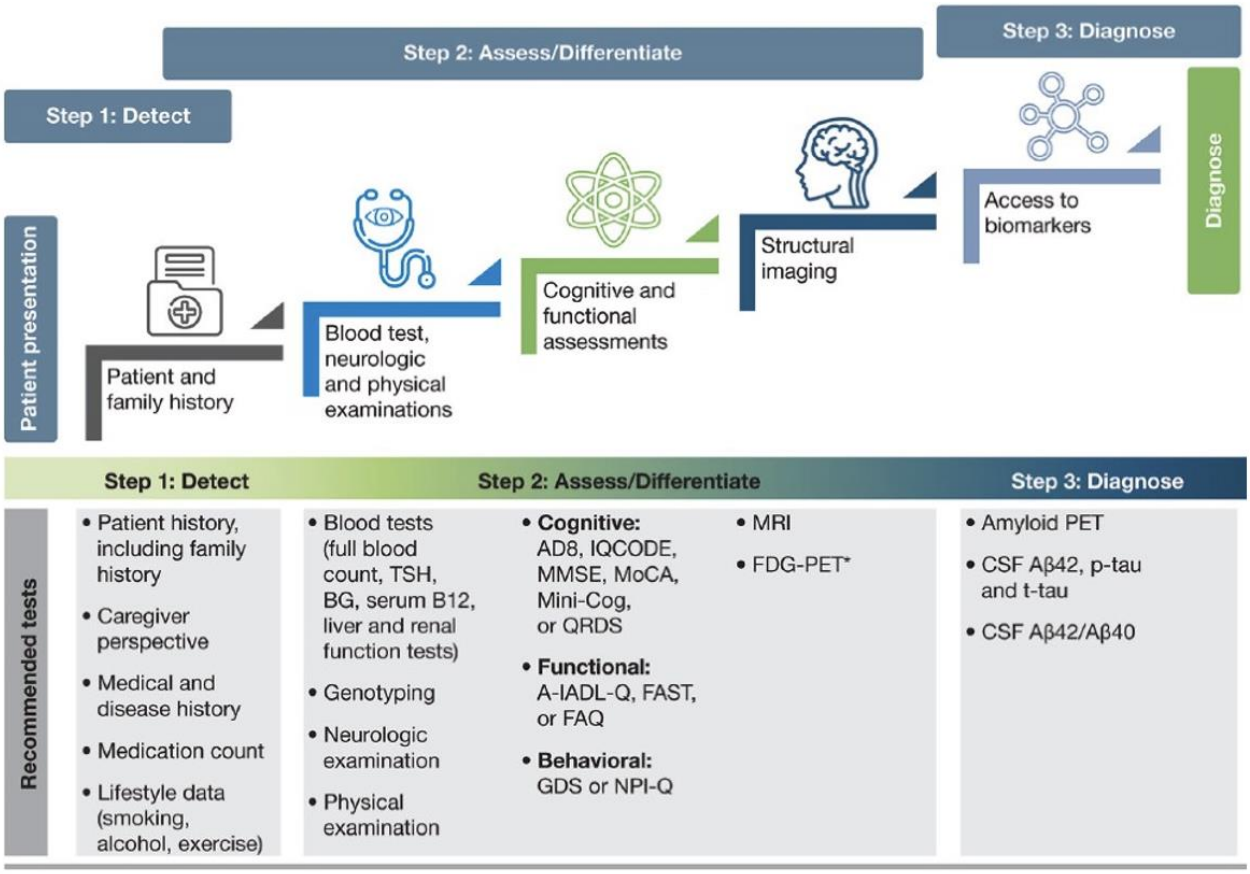

Fig. 2. Stages of the Diagnostic Process for Alzheimer's Disease [24]

The AT(N) framework has been created to classify and support the diagnosis of AD, using three key AD biomarkers [26]. "A" is aggregated Aβ or an associated pathological state, "T" denotes aggregated tau or tau-related pathological state, and "N" is neurodegeneration or neuronal injury. This AT(N) system indicates that AD should be diagnosed when both A and T biomarkers are abnormal, regardless of whether N biomarkers are also abnormal. In a case where A is found to be abnormal, while T and N remain normal, the condition should be classified as Alzheimer's pathologic change. If both A and N are abnormal but T is normal, the diagnosis is Alzheimer's disease, with concomitant suspected non-Alzheimer's pathologic change. All other biomarker patterns should be classified as non-AD pathological change [26].

1.1.2. Clinical features, pathology, treatment and diagnosis of frontotemporal dementia

FTD is a group of neurodegenerative disorders characterised by a progressive deterioration in behaviour, executive functioning, or language abilities. These disorders are associated with frontal and temporal lobe impairments. Among individuals younger than 65, FTD is one of the most common form of dementia. Compared to all age groups, FTD is the third most common type of dementia, following AD and LBD [27, 28]. FTD patients are characterised by more rapid progression and shorter life expectancy than individuals with AD. The average age of diagnosis for FTD is approximately 56, with most cases being diagnosed in people in their fifties. However, FTD can develop much earlier. About 13% of patients are diagnosed with this disorder before the age of 50, and there are cases where FTD is diagnosed in people in their twenties. In younger individuals and

especially in the early stages of the disease, the initial diagnosis of FTD is often misdiagnosed as a mental disorder, such as schizophrenia, bipolar disorder or depression [28].

Based on the symptoms that dominate in the disease, FTD is categorised into three primary syndromes. The most common type is behavioural variant FTD (bvFTD), which accounts for more than 50% of all FTD cases. On average, bvFTD develops at the age of 58. BvFTD is characterised by behavioural and personality changes, which include apathy, disinhibition, compulsive or repetitive behaviours, and hyperorality [29]. Each FTD syndrome is characterized by different patterns of neurodegeneration that affect specific brain regions, causing symptoms related to the functions of these regions. The bvFTD group (Figure 3A), compared with HC, shows reduced cortical thickness in the frontal and temporal cortices, as well as parts of the parietal lobe and cingulate cortex.

Another FTD syndrome is a non-fluent/agrammatic variant of primary progressive aphasia (nfvPPA). This FTD form is characterised by halting and grammatically impaired speech. Individuals diagnosed with nfvPPA often speak with inconsistent speech sound errors, which manifest as distortions, insertions, deletions, and transpositions of speech sounds. On average, nfvPPA develops at the age of 60 [29, 30]. The nfvPPA subtype (Figure 3B) is characterized by cortical thinning in the bilateral middle and superior frontal cortices, also in certain parts of the temporal cortex, and parietal regions.

Third FTD syndrome is the semantic variant of primary progressive aphasia (svPPA), which is defined by a gradual loss of semantic knowledge, i.e. understanding the meaning of words. Individuals diagnosed with svPPA experience a progressive decline in their ability to understand and remember the meaning of words and often exhibit dyslexia and dysgraphia [29]. The average age at which symptoms of svPPA appear is approximately 60 years [31]. The svPPA subtype (Figure 3C) shows reduced cortical thickness in several regions of the temporal cortex.

Frontotemporal lobar degeneration (FTLD) is the primary pathology of FTD, which is a group of neurodegenerative processes causing progressive neuron loss, gliosis and microvascular changes in the frontal and temporal lobes of the brain [27, 32]. FTLD is characterised by abnormal accumulation of specific intracellular proteins. The microtubule-associated protein tau in FTLD-tau, the transactive response DNA-binding protein 43 kD (TDP-43) in FTLD-TDP, and the fused in sarcoma protein (FUS) in FTLD-FUS are the main proteins involved in FTLD pathology [32]. When the disease starts to develop, misfolded proteins accumulate and selectively affect vulnerable neurons, disrupting their function. As the disease progresses, these pathological changes spread across wider networks in frontal and temporal cortices, causing the progressive behavioural and language impairment characteristic of FTD [33].

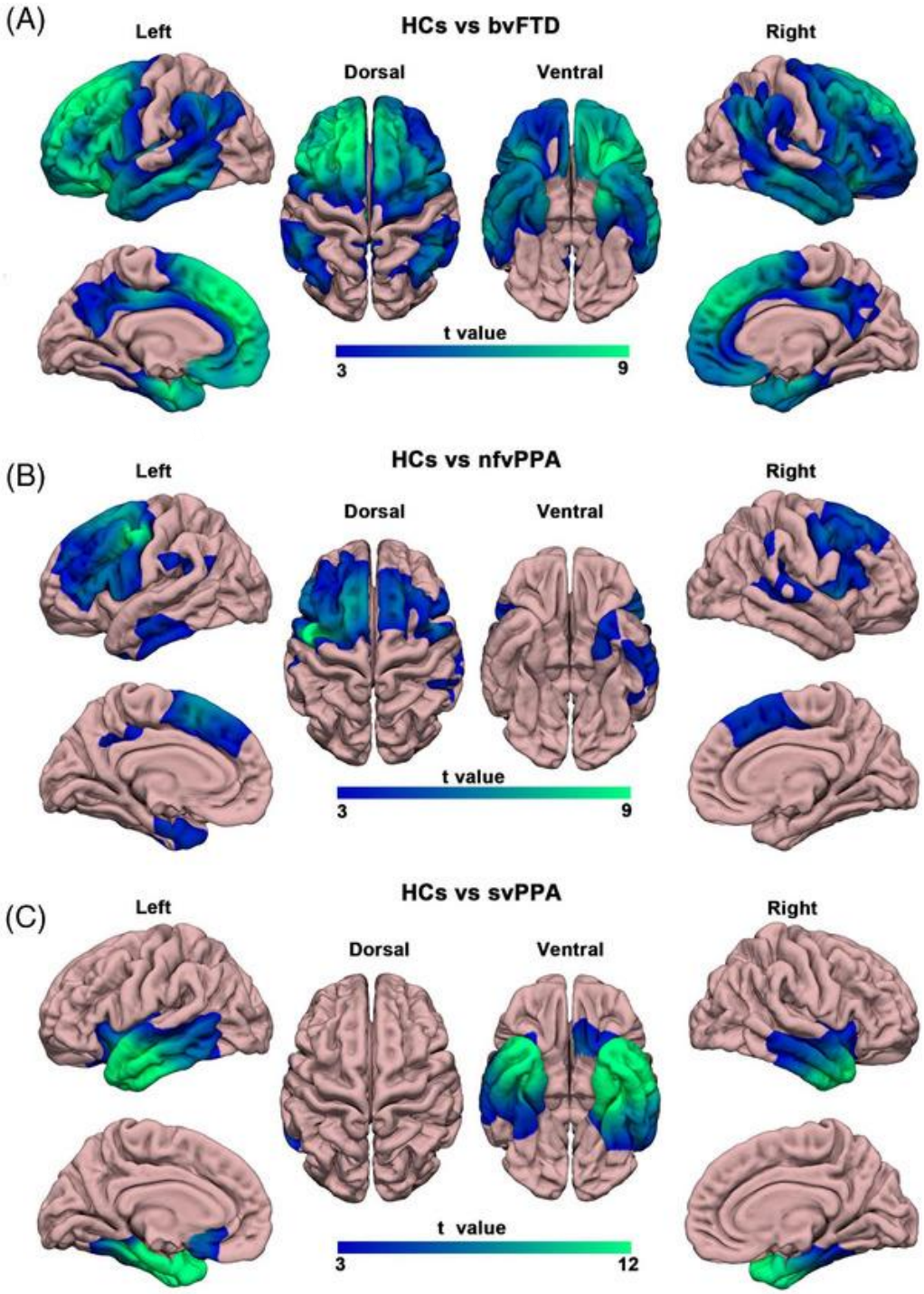

Fig. 3. Cortical Thinning Patterns in FTD Subtypes. Regions Showing Significant Cortical Reduction are Shown for bvFTD (A), nfvPPA (B), and svPPA (C) in Comparison with Healthy Controls (HCs) [34]

Unlike AD, there are currently no officially approved pharmacological treatments for FTD. Moreover, there is no evidence showing that drugs used for AD can help people with FTD, and in some cases they may even worsen the symptoms [35]. Nevertheless, it has been observed that certain pharmacological classes can mitigate some clinical symptoms. For example, selective serotonin reuptake inhibitors, which are widely used to treat depression and anxiety, have been shown to be effective in reducing behavioural symptoms such as disinhibition, irritability, and agitation. In more severe cases, atypical antipsychotics may be utilised, but they carry significant risks and must be used

with caution. In addition to pharmacological approaches, as in the case of AD, there are several non-pharmacological therapies that could be beneficial for individuals diagnosed with FTD. Most of these therapies are the same as for AD, but speech therapy has been identified as a particularly valuable therapeutic method for individuals with nfvPPA and svPPa subtypes [36, 37].

The diagnostic process for FTD is similar to that for AD. However, it is often more challenging due to the greater variability of early symptoms. The evaluation begins with detailed clinical assessment, during which information about patient's symptoms, medical, family history, and lifestyle is collected. Also, physical examination, blood tests are performed. Then, if necessary, cognitive screening tests, such as the MMSE or the Brief Cognitive Screening Battery (BBRC) are performed. For individuals with suspected language variants, a more detailed language assessment is performed. Furthermore, neuroimaging, such as CT or MRI, is utilised to determine whether there is atrophy in the frontal and/or temporal lobes. Functional imaging techniques help to assess changes in the brain metabolism and blood flow. For example, fluorodeoxyglucose (FDG) PET is used to evaluate cerebral glucose metabolism, while perfusion SPECT is used to measure cerebral blood flow. Additionally, specific AD biomarkers can be measured. However, these biomarkers are not used to diagnose FTD, but rather to help rule out AD when the diagnosis is unclear. In such cases, AD-specific CSF biomarkers (e.g. Aβ42, t-tau, p-tau) are used [38, 39]. Furthermore, genetic factors play an important role in FTD, with up to 40% of patients reporting a family history of a similar disorder. Therefore, genetic testing is often included in the diagnostic process [40].

Current AD and FTD diagnostic methods, which use neuroimaging, biomarkers and genetic testing can achieve high diagnostic accuracy. However, they are expensive, time-consuming and not accessible to everyone [6]. Due to these limitations, it is sometimes difficult to diagnose the disease in time, which complicates treatment, as early detection of neurodegenerative diseases is essential for effective symptom management. Therefore, there is a need for more affordable and widely accessible diagnostic method.

1.2. Overview of electroencephalography

EEG is a non-invasive technique used to measure the electrical activity of the brain [41]. When an EEG is recording, multiple electrodes are placed on the scalp to measure potential differences between electrode pairs, thereby capturing the sum of postsynaptic potentials generated by many cortical pyramidal neurons. The main source of the EEG signal is the cerebral cortex, as its neurons are closest to the scalp [42]. EEG does not reflect the activity of individual neurons or isolated cortical regions, instead, it represents the combined electrical activity of many neurons working together [43]. Consequently, EEG provides a macroscopic perspective on brain function, offering insight into large-scale neural dynamics.

EEG signals are complex, non-linear and non-stationary. For this reason, many feature extraction techniques have been developed for EEG analysis. For example, one widely used technique divides the EEG signal into frequency bands defined as delta, theta, alpha, beta and gamma [6]. To extract this frequency information, Fourier-based computational methods are commonly used. These often include Welch's power spectral density (PSD) [44] or Fast Fourier Transform (FFT) [45]. Each frequency band represents a different frequency range and is linked with specific cognitive functions (Figure 4). The delta band (0.5–4 Hz) is most noticeable during the stage of deep sleep. This low frequency band is associated with restorative processes and brain recovery. The theta band (4–8 Hz)

is linked with memory encoding, drowsiness, and the initial phase of sleep. The alpha band (8–12 Hz) is associated with a relaxed, closed-eyes, awake state. The beta band (12–30 Hz) is linked with active thinking and motor control. Beta band activity typically increases during tasks that require focused attention or movement. The gamma band (30–100 Hz) is related to higher-order cognitive processes, including attention, perception, and the integration of sensory information [6, 46]. Previous studies show that these frequency patterns change in people with neurodegenerative disorders. For example, study [47] reported that increased theta band spectral power and decreased alpha band spectral power were found in most cortical regions in individuals with AD compared with HC.

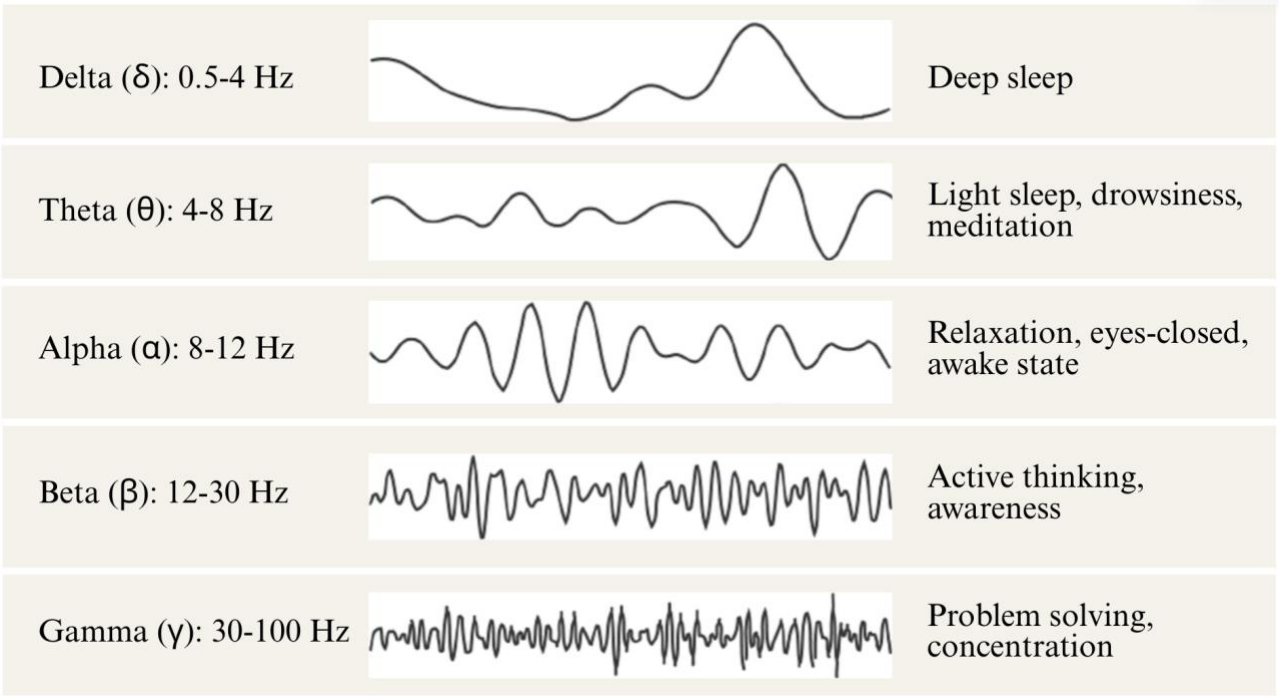

Fig. 4. Frequency Bands of EEG Signal and Their Associated Cognitive States. Adapted from [48]

Another common EEG feature extraction technique is functional connectivity (FC). It shows how different regions coordinate their activity by evaluating correlations between spatially separated signals over time. FC can be calculated by various methods, such as Pearson's correlation, coherence, phase lag index (PLI) and others. In healthy individuals, connections between different parts of the brain are relatively similar, however the strength of these connections changes in patients with neurodegenerative diseases. Recent study [49] reported that both AD and FTD patients showed abnormal connectivity patterns. They found significant increase in whole-brain PLI in the theta band, and significant decrease in whole-brain PLI in the alpha band. Similarly, another study [50] found that AD patients exhibited reduced coherence in the alpha band. These results confirm FC changes in individuals with neurodegenerative disorders, which provides opportunities for further investigation and the development of new diagnostic methods.

EEG is a non-invasive, affordable, and widely accessible technique with excellent temporal resolution. Although its spatial resolution is lower than several other neuroimaging methods such as MRI, EEG remains highly valuable due to its many advantages [47]. Over the past decade, EEG has been widely investigated as a clinical tool for the detection, monitoring, and assessment of various neurological conditions, including epilepsy [51], Parkinson's disease [52], and even emotional or psychiatric conditions [53]. Moreover, there is growing interest in applying EEG analysis to

neurodegenerative disorders. Additionally, various machine learning (ML) techniques have made it much easier and faster to analyse complex EEG data, offering promising opportunities to improve diagnostic accuracy and support clinical decision-making.

1.3. Background on EEG classification of AD and FTD

Various studies, employing different methods, have classified AD and/or FTD patients from HC. For example, study [6] proposed a deep learning approach for the classification of individuals diagnosed with AD, FTD and HC subjects, using EEG signals. Researchers used advanced preprocessing techniques with a convolutional neural network (CNN) trained on FFT-based heatmaps. These heatmaps showed EEG signal power distribution across frequencies for each of the 19 channels. The proposed CNN model with leave-N-subjects-out (LNSO) validation, achieved an accuracy of 79.45% for distinguishing AD from HC, 72.85% for FTD vs. HC classification, and 80.69% for the combined AD+FTD vs. HC classification. Another study [54], computed time-domain features (mean, variance, interquartile range) and frequency-domain features (delta, theta, alpha, beta, gamma power) for each of the 17 EEG channels and used these features as input for classification. The classification was performed using multiple ML models, and the performance was evaluated using leave-one-subject-out (LOSO) cross-validation. The best performance was achieved using decision trees with an accuracy of 78.5% for AD vs. HC classification and random forests with an accuracy of 86.3% for FTD vs. HC classification. Another recent study [55] created time-frequency FC (TF-FC) and band-pass filtered FC (BF-FC) matrices using Pearsons's correlation, mutual information and PLI. Only the most important features were selected and used as input to an SVM classifier with leave-one-out (LOO) cross-validation. Researchers reported that employing the top 20 TF-FC features the model achieved 95.38% accuracy for distinguishing between AD and HC. Using the top 50 TF-FC features allowed the model to achieve accuracy of 89.77% for classifying combined AD+FTD from HC. Utilising the top 10 BF-FC features SVM classifier achieved 84.62% accuracy for FTD vs. HC. All of these results confirm that relatively high classification performance for distinguishing AD and/or FTD from HC can be achieved using various extracted EEG features and ML methods. Therefore, EEG has the potential to be an effective diagnostic method for neurodegenerative disorders.

However, distinguishing between the dementia subtypes remains particularly challenging. It has been determined that about 36% of AD cases cannot be differentiated from FTD using standard diagnostic methods. This is because more than half of patients with atypical AD meet the criteria for FTD, due to overlapping symptoms such as apathy. Also, many individuals with FTD complain about memory impairment and meet the diagnostic criteria for AD [38]. While certain imaging techniques and fluid biomarkers can help distinguish between the disorders, these diagnostic tools are expensive and not widely accessible. Therefore, further investigation into EEG recordings and brain network activity is necessary, as this could lead to the development of more accessible and affordable differential diagnostic methods.

Several studies have investigated the use of EEG signals for distinguishing AD from FTD, but research in this area remains limited. Study [54] used time-domain and frequency-domain features as input for several ML models and evaluated them with LOSO cross-validation. The best performance for differentiating AD from FTD was obtained utilising SVM classifier (68% accuracy, SD = 18) and decision trees (73% accuracy, SD = 11). Study [6] used FFT-based heatmaps as input for a CNN, and performed multiclass classification of AD, FTD and CN. Using LNSO validation, the model achieved an overall accuracy of 54.28% with individual F1 scores of 57.00% for AD, 66.98% for HC, and

23.54% for FTD. Another study [56] achieved the highest performance of all previous studies utilising PHI connectivity values for classification. 13 electrode pairs, age and gender were used as features, resulting in an input set of 15 features. Using the LOO cross-validation, the SVM model reached 91.5% accuracy in differentiating between AD and FTD. Moreover, this performance was improved to 96.6% by reducing the feature set to the 8 most important features.

Recent studies have shown the potential of using non-invasive EEG recordings to differentiate between AD and FTD. Nevertheless, current findings are still limited. Therefore, further research is necessary to identify the most informative EEG features and to develop a model that would have accuracy and reliability needed for clinical practice. In this study, spectral analysis was performed to examine whether AD and FTD differ in their EEG frequency characteristics. The FC was computed using Pearson's correlation and coherence. These connectivity features, both combined and individually, were used as input to a CNN model for the classification of AD and FTD. Finally, the most important features contributing to the classification were extracted to identify connections with the highest diagnostic relevance.

2. Data and methodology

2.1. Dataset description

The dataset used in this study was obtained from OpenNeuro, publicly available online repository [57]. This dataset consisted of closed-eyes, resting-state EEG recordings from 59 participants, of whom 36 individuals were diagnosed with AD and 23 with FTD. The median disease duration is 25 months, with an interquartile range of 24-28.5 months [57]. Table 1 presents the gender distribution, mean age and average MMSE scores of the participants. The AD group consists of 12 males and 24 females, with an average age of 66.39 years (SD = 7.89). The FTD group comprised 14 males and 9 females, with an average age of 63.65 years (SD = 8.22). The data also includes MMSE scores for each participant. The MMSE is a paper-based test that evaluates orientation, attention, concentration, verbal memory, naming ability, and visuospatial skills, with scores ranging from 0 to 30. Higher scores indicate better brain functioning, lower scores are associated with an impairment [6, 8]. The mean MMSE value for the AD group was 17.75 (SD = 4.50) and for the FTD group was 22.17 (SD = 2.64).

Table 1. Demographic and Clinical Characteristics of the Alzheimer's Disease and Frontotemporal Dementia Groups

Group	***N***	**Gender (Male/Female)**	**Age (Mean ± SD)**	**MMSE (Mean ± SD)**
AD	36	12/24	66.39 ± 7.89	17.75 ± 4.50
FTD	23	14/9	63.65 ± 8.22	22.17 ± 2.64

Electrical signals were recorded from 19 scalp electrodes, which were positioned according to the 10-20 international system (Figure 5). The signals were recorded at a sampling rate of 500 Hz, with a resolution of 10 μV/mm. The mean duration of the recordings was approximately 13.5 min for the AD group (ranging from 5.1 to 16.5 min) and approximately 12 min for the FTD group (ranging from 7.9 to 16.9 min).

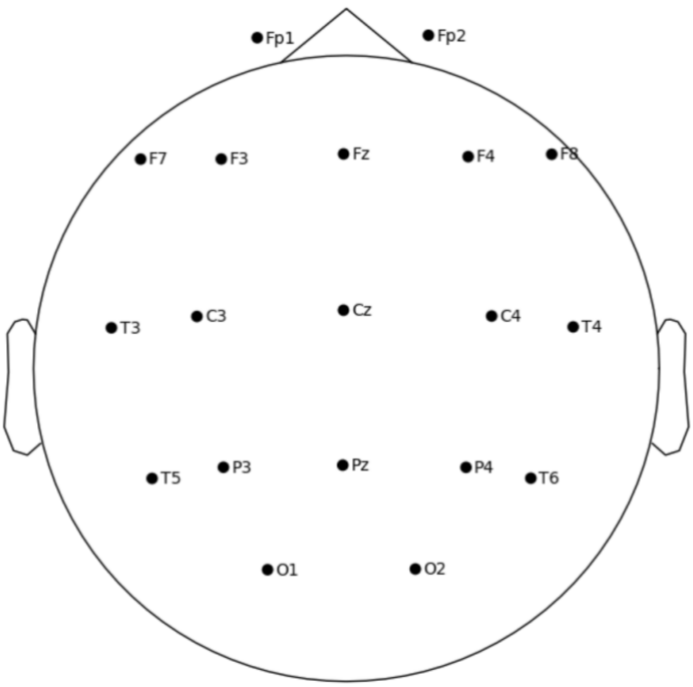

Fig. 5. Scalp Electrode Locations in the 10-20 EEG System

The dataset used in this work was obtained in a preprocessed form. In the preprocessing pipeline, the EEG signals were re-referenced to the average of A1-A2 and filtered using a Butterworth band-pass filter between 0.5 and 45 Hz. The data was then processed through an Artifact Subspace Reconstruction (ASR) procedure, which automatically removed segments containing large or persistent artefacts by applying a conservative threshold corresponding to a 0.5 s window standard deviation of 17. Subsequently, Independent Component Analysis (ICA) was performed using the RunICA algorithm to decompose the 19-channel EEG into 19 independent components. Components that were identified as eye- or jaw-related artefacts by the ICLabel automatic classifier in EEGLAB were subsequently removed [57].

2.2. Methods

2.2.1. Overall workflow

This project began with EEG data preprocessing, after which two types of features were extracted. Firstly, spectral features were analysed to determine the differences in spectral power between AD and FTD, and to identify the frequency ranges in which the difference between the groups was greatest. Subsequently, FC was analysed by calculating Pearsons's correlation and coherence from the time domain EEG signals. These FC features were used for CNN-based classification, and the performance was compared with an SVM classifier. Finally, the most important input features for the CNN classification were identified using a saliency-based analysis. The complete workflow is illustrated in Figure 6.

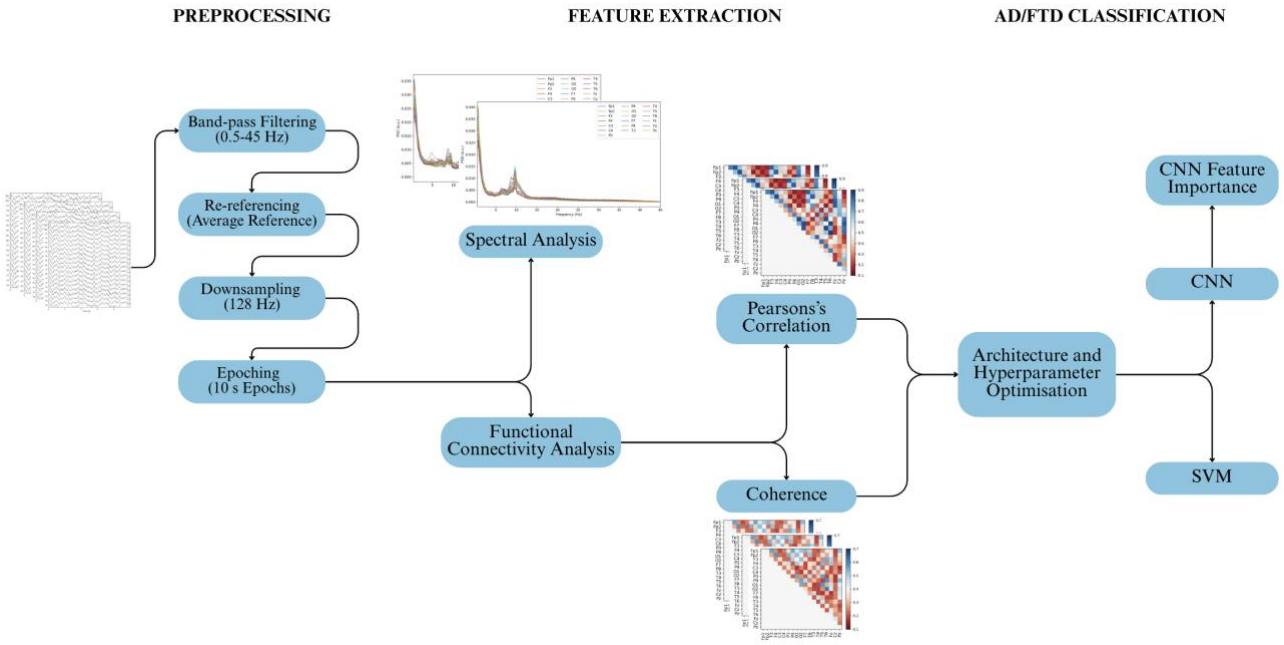

Fig. 6. Workflow of the Project

2.2.2. Data preprocessing

The initial step in the analysis was to additionally preprocess the dataset. A Butterworth band-pass filter with a bandwidth ranging from 0.5 to 45 Hz was utilised to filter the data. Then, the data was

re-referenced to the average, and down-sampled to 128 Hz. Subsequently, the recordings of all individuals were segmented into 10 s epochs. Each epoch consisted of 1281 time points, corresponding to 10 s segments sampled at 128 Hz. The artifact-cleaning procedure introduced "boundary" events, which are markers indicating discontinuities, where parts of the signal had been removed. Therefore, epochs containing "boundary" events were excluded from further analysis. It is important to note that the total number of 10 s epochs differs among participants due to variations in recording duration and the number of "boundary" events. In the AD group, the number of remaining epochs ranged from 29 to 121, with an average of 76 epochs (SD = 16.33). In the FTD group, the number of epochs ranged from 22 to 94, with an average of 67.61 (SD = 16.25). It was assumed that these epoch number variations across participants will not have a significant impact on the analysis, as features derived from each epoch will be either averaged or used individually during model training/testing. Figure 7 demonstrates a segment of EEG recording from an AD subject before and after preprocessing.

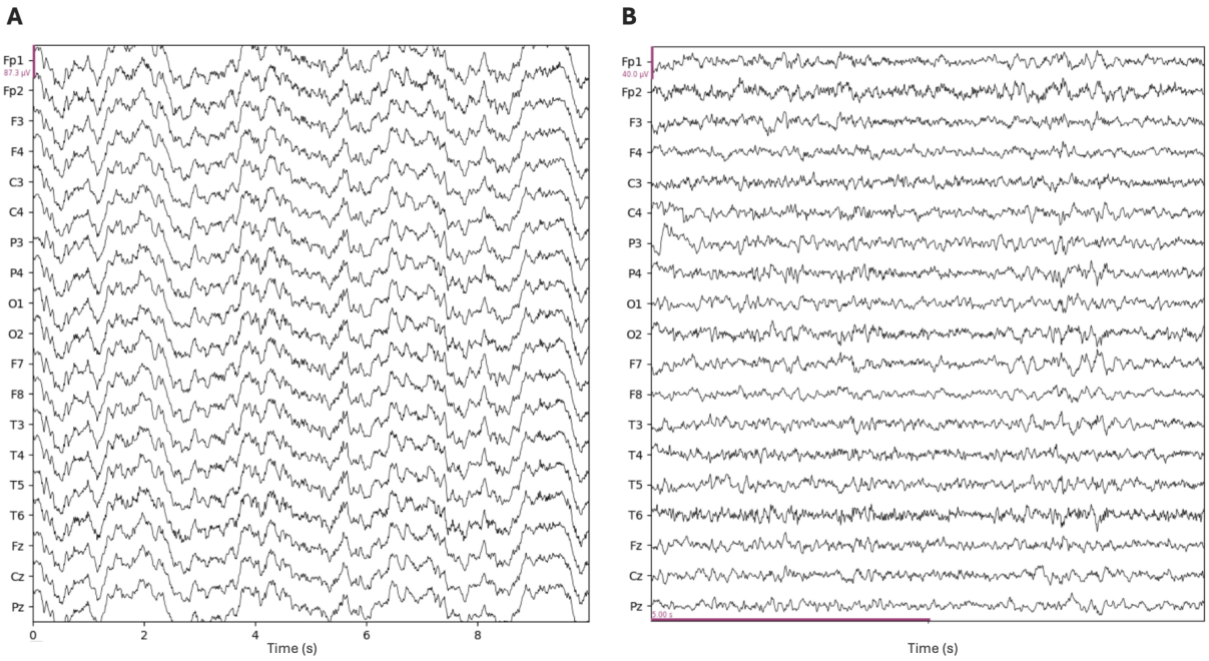

Fig. 7. EEG Segment Before Preprocessing (A) and the Corresponding Preprocessed 10 s Epoch (B) From the Same Alzheimer's Disease Subject

2.2.3. Spectral feature extraction

Spectral features from the EEG recordings were extracted by transforming each epoch from the time domain into the frequency domain using the FFT, which is an efficient computational implementation of the Discrete Fourier Transform (DFT). In comparison with the DFT, which has a computational complexity of $O(n^2)$, the FFT significantly reduces computational time to $O(n \log n)$ [45]. The DFT is defined as:

$$X_k = \sum_{n=0}^{N-1} x_n e^{-\frac{2\pi i k n}{N}} \quad k = 0, \ldots, N-1 \tag{2.1}$$

where X_k represents the k^{th} coefficient of the DFT, N is the number of discrete time points in the epoch, x_n is the input signal at the time domain, and $i = \sqrt{-1}$.

Before the Fourier Transform was applied, each EEG epoch was mean-centred to remove the DC offset. For each channel, the mean value of the signal across the epoch was subtracted from each value, which can be expressed as follows:

$$y_k = x_k - \frac{1}{N}\sum_{n=0}^{N-1} x_n \tag{2.2}$$

where y_k is the mean-centred signal, and x_k is the original EEG value at time index *k*.

Additionally, the Hann window was applied to smooth the signal at the boundaries [58]. The Hann window is defined as follows:

$$w_k = 0.5 - 0.5\cos\left(\frac{2\pi k}{N-1}\right) \tag{2.3}$$

The windowed signal was then obtained by multiplying the mean-centred signal with the Hann window:

$$z_k = y_k w_k \tag{2.4}$$

The windowed Fourier transform was computed according to:

$$X_k = \sum_{n=0}^{N-1} z_n e^{-2\pi jkn/N} \tag{2.5}$$

Subsequently, the PSD was calculated using the resulting Fourier coefficients [44]. The PSD for each frequency bin was calculated as follows:

$$P_k = \frac{|X_k|^2}{U} \tag{2.6}$$

where *U* is window normalisation factor, defined as:

$$U = \frac{1}{N}\sum_{n=0}^{N-1} |w_n|^2 \tag{2.7}$$

The final step was the normalisation of the PSD by dividing each frequency bin by the total spectral power:

$$PSD_k = \frac{P_k}{\sum_n P_n} \tag{2.8}$$

The normalisation ensured that each PSD value reflected the proportion of total power contained in that frequency bin, allowing for comparison across subjects and epochs, even when their absolute signal amplitudes differed.

2.2.4. Statistical analysis

The following procedure was applied to determine whether there was a statistically significant difference between the AD and FTD groups in their averaged PSD values (averaged across subjects

and channels) across the theta band, the alpha band and the combined 4–12 Hz frequency range. Shapiro–Wilk test was employed to ascertain whether the values in each group were normally distributed, followed by Levene's test to evaluate the homogeneity of variances. For the data that did not violate the assumptions of normality and equal variance, a two-sided independent samples t-test was performed to determine whether the groups differ significantly. Two-sided Mann-Whitney U test was applied to the data that were not normally distributed. If the p-value was less than 0.05, the difference was considered to be significant. Also, the same statistical procedure was used to compare MMSE scores between the AD and FTD groups.

2.2.5. Functional connectivity analysis

For FC analysis, two classical measures were used: Pearson's correlation and coherence. Pearson correlation quantifies FC between EEG channel pairs, measuring how similarly two signals change over time, indicating the strength of their linear relationship [59]. The correlation coefficient ranges from –1 to 1, where values close to –1 indicate a strong negative linear relationship, values near 0 indicate no linear relationship, and values close to 1 indicate a strong positive linear relationship. For two *x* and *y* signals, the Pearson's correlation is defined as follows:

$$r_{xy} = \frac{\sum_{n=0}^{N-1}(x_n - m_x)(y_n - m_y)}{\sum_{n=0}^{N-1}(x_n - m_x)^2 \sum_{n=0}^{N-1}(y_n - m_y)^2} \tag{2.9}$$

where m_x and m_y are the means of *x* and *y* signals.

Coherence is another commonly used FC measure. It quantifies how consistently two EEG signals oscillate together at specific frequencies, reflecting the stability of their linear relationship in both amplitude and phase. Unlike correlation, which evaluates similarity in the time domain, coherence is frequency-specific measure, which indicates how strongly two brain regions are synchronised at a specific frequency. The coherence values ranges from 0, indicating no consistent relationship, to 1, indicating a perfect linear relationship [59]. The coherence between two *x* and *y* signals is defined as follows:

$$C_{xy}(f) = \frac{\left|P_{xy}(f)\right|^2}{P_{xx}(f)P_{yy}(f)} \tag{2.10}$$

where *f* is the frequency, $P_{xy}(f)$ is the cross-spectral density between the two signals, $P_{xx}(f)$ and $P_{yy}(f)$ are their respective auto-power spectral densities.

Pearson correlation and coherence were calculated for each EEG epoch, for the theta (4–8 Hz) and alpha (8–12 Hz) frequency bands. Initially, the EEG epochs were band-pass filtered, after which Pearson correlation or coherence was calculated between all pairs of channels. For example, the EEG recording was band-pass filtered with a bandwidth ranging from 4 to 8 Hz, then Pearson correlation coefficients were computed between all channels, resulting in the theta band Pearson correlation matrix. Due to the symmetry of correlation matrices, only the values in the upper-right triangle (excluding the diagonal) were kept. All other matrix values were set to zero to remove redundant information. Then each resulting connectivity matrix was used for model training and testing. Furthermore, in order to compare group-level patterns, the epochs were averaged across each subject,

and then averaged across subjects in each group. To achieve clearer visual comparison, the group-averaged matrices for AD and FTD were subtracted from one another.

Aditionally, for the comparison of several selected subjects, Pearson correlation was calculated between their flattened, subject-averaged connectivity matrices to assess their similarity.

2.2.6. Convolutional neural network architecture search

The classification of AD and FTD FC matrices was implemented using a CNN. CNNs are supervised deep learning algorithms capable of processing images, learning the most relevant features through its weights and biases, and identifying different classes based on those learnt patterns [60]. Initially, an architecture search was performed, to identify the most effective model architecture. In this step, the theta and alpha bands Pearson correlation matrices were used as the input features (Figure 8). The input shape was 19 × 19 × 2, where one channel corresponds to the theta band Pearson correlation matrix and the other to the alpha band Pearson correlation matrix.

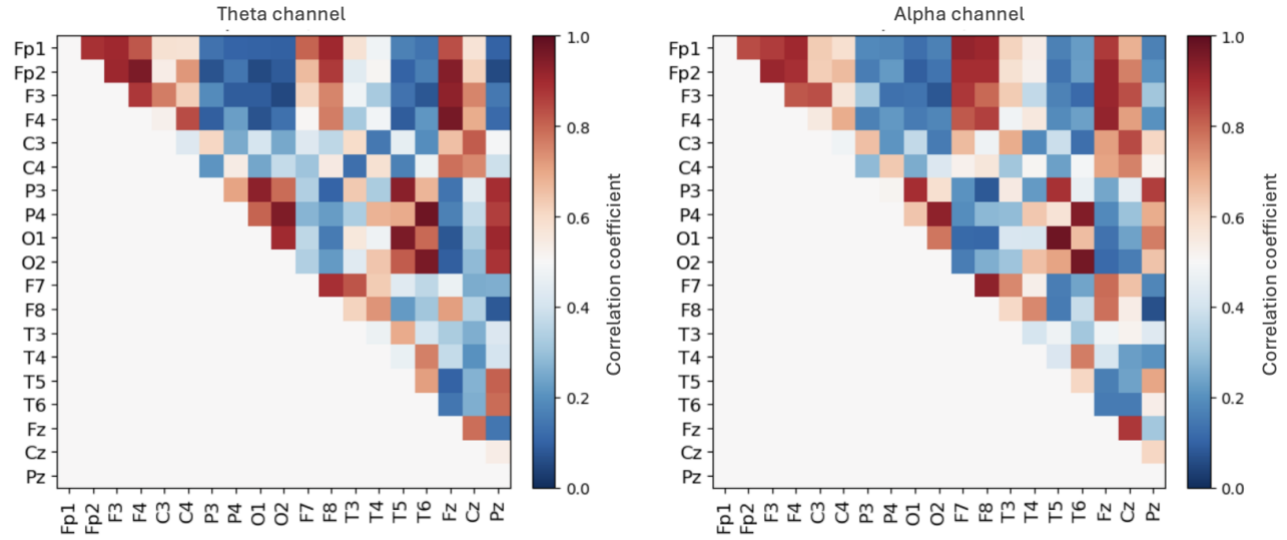

Fig. 8. Input Correlation Matrices (Theta and Alpha Bands) From a Single EEG Epoch Used for the CNN Architecture Search

The dataset consisted of 4291 theta-alpha matrix pairs, derived from all epochs of the 59 subjects. Before the model's training, both the theta and alpha Pearson correlation matrices were min–max normalised to the range from 0 to 1. The dataset was then subject-wise divided into training, validation, and test sets, with a ratio of 70/15/15. This resulted in a total of 2983 samples in the training set, 600 in the validation set, and 708 in the test set. Before the training process, each set was separately standardised using the mean and standard deviation of the training set, according to the following equation:

$$X_{std} = \frac{X - \mu_{train}}{\sigma_{train}} \tag{2.11}$$

A wide range of convolutional neural network architectures were investigated, including models with one, two, and three convolutional layers, different numbers of filters (8, 16, 32, 64, 128), and the additional dense layer. Also, the exploration of batch normalisation, max-pooling layers (applied in both combination and individually), and dropout layers applied between the convolutional blocks and

the flatten layer. During this search, all models were trained using the same hyperparameters: Adam optimiser with a learning rate of 0.001, a batch size of 16, and 30 training epochs.

After the selection of the best architecture, a hyperparameter search was conducted for that model. Several learning rates (0.01, 0.0001), batch sizes (8, 32), and dropout rates (0.2, 0.6) were evaluated.

The pilot tests demonstrated some variability between training iterations of the same architecture. Therefore, each model configuration was trained and evaluated five times. The mean accuracy across five runs was calculated and used to compare architectures and select the best model. The results of the CNN architecture search are reported in Appendix 1 Table 4.

The architecture that achieved the best performance (Figure 9) was selected for further evaluation with different input configurations. Depending on the data provided to the network, the model's input shape was either 19 × 19 × 1, 19 × 19 × 2 or 19 × 19 × 4. The selected architecture starts with a convolutional layer consisting of 64 filters of size 3 × 3, using padding and a ReLu activation function to introduce non-linearity. Subsequently, a Batch Normalisation layer is employed to stabilise the training process. The second convolutional layer contains 128 filters with the same 3 × 3 kernel size, with padding and ReLu activation function, followed by another Bach Normalisation layer. The third convolutional layer employs 256 filters with 3 × 3 kernels, padding and ReLu activation function with subsequent Bach Normalisation. Following the convolutional layers, a Flatten layer transforms the multi-dimensional feature maps into one-dimensional vector. A dropout layer with a rate of 0.4 is then applied to reduce overfitting. Finally, the model concludes with a Dense output layer with a single unit and a sigmoid activation function, which gives a probability value for binary classification.

Layer (type)	Output Shape	Param #
conv2d_8 (Conv2D)	(None, 19, 19, 64)	640
batch_normalization_6 (BatchNormalization)	(None, 19, 19, 64)	256
conv2d_9 (Conv2D)	(None, 19, 19, 128)	73,856
batch_normalization_7 (BatchNormalization)	(None, 19, 19, 128)	512
conv2d_10 (Conv2D)	(None, 19, 19, 256)	295,168
batch_normalization_8 (BatchNormalization)	(None, 19, 19, 256)	1,024
flatten_4 (Flatten)	(None, 92416)	0
dropout_6 (Dropout)	(None, 92416)	0
dense_6 (Dense)	(None, 1)	92,417

Total params: 463,873 (1.77 MB)
Trainable params: 462,977 (1.77 MB)
Non-trainable params: 896 (3.50 KB)

Fig. 9. Summary of the Selected CNN Model Architecture and Layer Parameters for a (19 × 19 × 1) Input

2.2.7. Classification using a convolutional neural network

The performance of the selected CNN model was evaluated using LOSO cross-validation. LOSO is a validation technique, where the model is trained on all subjects except one, with the remaining subject being used for testing. This process is repeated until all subjects have been once used as the test subjects. LOSO validation technique ensures that model performance is assessed on completely unseen subjects and minimises bias due to subject-level variability [61]. In this project, LOSO validation was applied using nine different input configurations to determine the most effective features set for differentiating between AD and FTD. Depending on the experiment, the model input consisted of either one (19 × 19 × 1) or two (19 × 19 × 2), or four channels (19 × 19 × 4). The following inputs were included:

- Combined theta and alpha Pearson correlation matrices (19 × 19 × 2), as well as each band separately (only theta, only alpha 19 × 19 × 1).
- Combined theta and alpha coherence matrices (19 × 19 × 2), and each band separately (only theta, only alpha 19 × 19 × 1).
- Combined Pearson correlation and coherence input, including both bands (19 × 19 × 4), only the theta band (19 × 19 × 2) and only the alpha band (19 × 19 × 2).

Before model's training, the absolute values of the Pearson correlation matrices were calculated to ensure that the connectivity magnitudes were on the same scale as coherence. As coherence values naturally range from 0 to 1, no additional normalisation was applied to them. Furthermore, after the data division for each LOSO cross-validation fold, the training and test sets were standardised separately using the mean and standard deviation that had been computed from the training data.

A total of 4291 inputs were prepared for the training and testing. For each LOSO iteration, the matrices corresponding to the left-out subject were assigned to the test set, while the remaining matrices were utilised for training. The training process was conducted using the Adam optimiser with a learning rate of 0.001, a batch size of 16, and 30 training epochs, along with early stopping to prevent overfitting. Binary cross-entropy was defined as loss function. For the model's evaluation, accuracy scores obtained from all LOSO validation folds were averaged to obtain the final performance estimate.

2.2.8. Classification using support vector machine

A support vector machine (SVM) classifier was performed for the comparison of classification performance with CNN. SVMs are supervised learning algorithms that are utilised for the regression and classification tasks. The underlying principle of SVMs is to determine the optimal separating hyperplane that best divides data points belonging to different classes in a multidimensional feature space [55]. In this study, hyperparameter tuning was performed using the same theta and alpha Pearson correlation matrices that were used during the CNN architecture search. In order to optimise the SVM classifier, a grid search was conducted. Both radial basis function (RBF) and linear kernels were evaluated. Several values (0.001, 0.01, 0.1, 1, 10, 100) for the regularisation parameter C were tested for each kernel. The gamma parameter was tuned using the values 'scale', 0.001, 0.01, 0.1, and 1, for the RBF kernel. After this search, the optimal configuration was found to be an RBF kernel with gamma set to 'scale' and C set to 0.1.

Using these hyperparameters, the SVM was evaluated with LOSO cross-validation across all nine input configurations. The preprocessing pipeline remained identical to that used for the CNN models:

Pearson correlation matrices were converted to their absolute value, while coherence matrices remained unchanged. Following each LOSO validation split, the train and test sets were standardised separately using statistics calculated from the training data. This ensured a fair and consistent comparison between the CNN and SVM classification performances. The final SVM performance was obtained by averaging the classification accuracies across all LOSO cross-validation folds.

2.2.9. Saliency-based feature importance estimation

Saliency maps were computed to determine which input features contribute most to the CNN's classification [62]. Particularly, gradient-based input saliency was used. It is a technique, which identifies the input matrix parts that have the greatest influence on the output of the model. This method evaluates the model's prediction sensitivity to small changes in each input value [63]. The gradient of the model's output score with respect to each input was computed:

$$g = \frac{\partial S}{\partial x} \tag{2.12}$$

where S is the model's output score for the predicted class and x is the input matrix.

To have saliency maps that are more stable and less noisy, the Gradient ⊙ Input saliency method was employed [64]. The Gradient ⊙ Input saliency value is computed by the element-wise product of the input and the gradient:

$$Saliency = x \odot \frac{\partial S}{\partial x} \tag{2.13}$$

2.2.10. Experimental setup

The MNE [65] library was used for data importation and preprocessing. The implementation of the Fourier transform and FC measures were using the SciPy [66] library, with the real-valued FFT used for spectral analysis. The CNN models were created and fitted using the TensorFlow [67], and the SVM classifier was implemented using Scikit-learn [68]. All experiments were conducted in Python [69] in the Jupyter Notebook, with additional support of NumPy [70], pandas [71], Matplotlib [72], Scikit-learn [68] and Seaborn [73] libraries for mathematical computation, data handling and visualisation.

3. Results and discussion

3.1. Cognitive performance differences between AD and FTD

A comparison of MMSE between individuals diagnosed with AD and FTD revealed that these groups have significantly different scores (Figure 10). Patients with AD exhibit lower MMSE scores (mean = 17.75) compared with FTD (mean = 22.17). This difference could be due to the fact that AD patients typically experience early memory and orientation impairments. These functions are most strongly assessed by the MMSE test [74]. In contrast, FTD is characterised by more pronounced behavioural or language disturbances, while general cognitive performance may remain relatively unimpaired in the early stages of the disease, resulting in higher MMSE score.

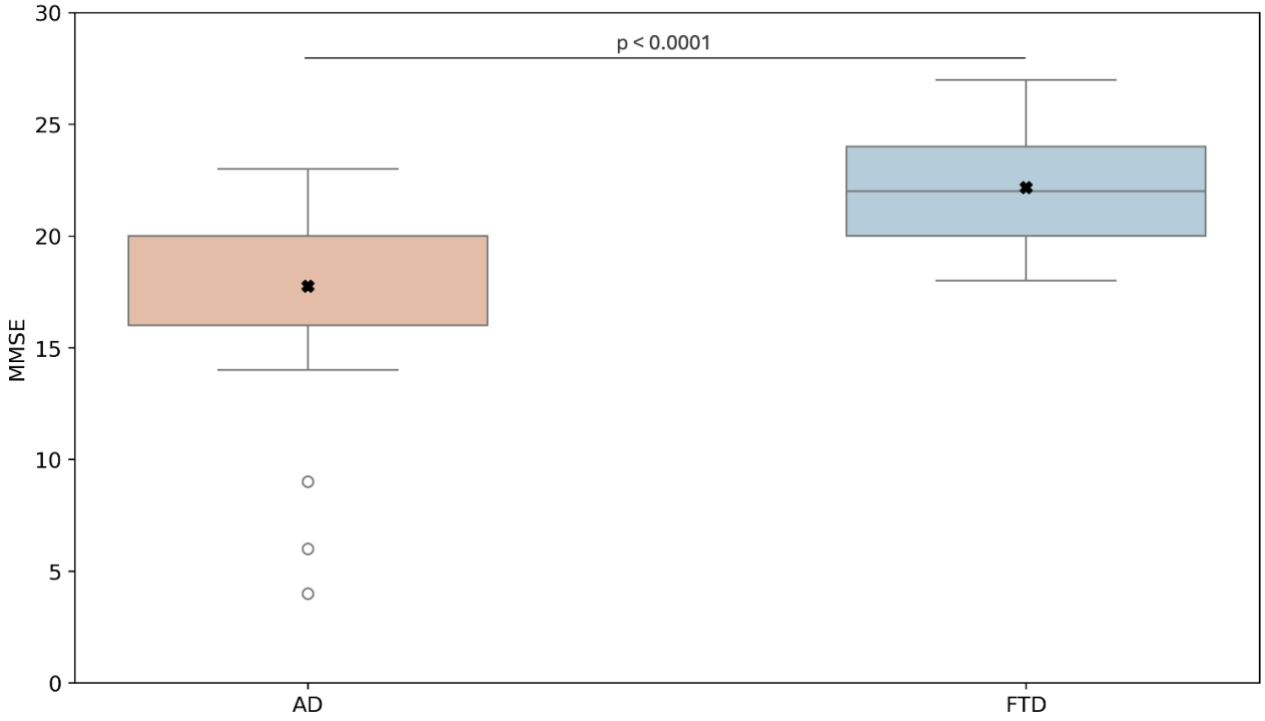

Fig. 10. Distribution of MMSE Scores for Alzheimer's Disease and Frontotemporal Dementia Patients (× represents the mean)

3.2. Spectral analysis results

For spectral comparison between the groups and channels, the PSD values were averaged across the subjects. To provide a clearer view of the spectral distribution across the EEG channels, the results were visualised using both line charts (Figure 11A, C) and heatmaps (Figure 11B, D). In the delta band, a larger number of channels show higher PSD values in the FTD group (Fp1, Fp2, F3, F4, P3, P4, O1, O2, F7, F8, Fz, Cz, Pz) compared with the AD group (Fp1, Fp2, F7, F8). In the theta band, the AD group shows a noticeably higher peak at the Fz channel compared to the other channels in this frequency range.

Furthermore, the AD group tends to show a reduced alpha peak across most channels. This reduction is most noticeable in the occipital (O1, O2) and posterior temporal (T5, T6) regions when compared with the FTD. However, in both groups, alpha activity appears to be distributed across broader cortical areas rather than being localised to the occipital and posterior temporal regions, as typically

observed in healthy individuals. This widespread alpha activity suggests disrupted connectivity and neural networks desynchronization, which are often observed in neurodegeneration [6].

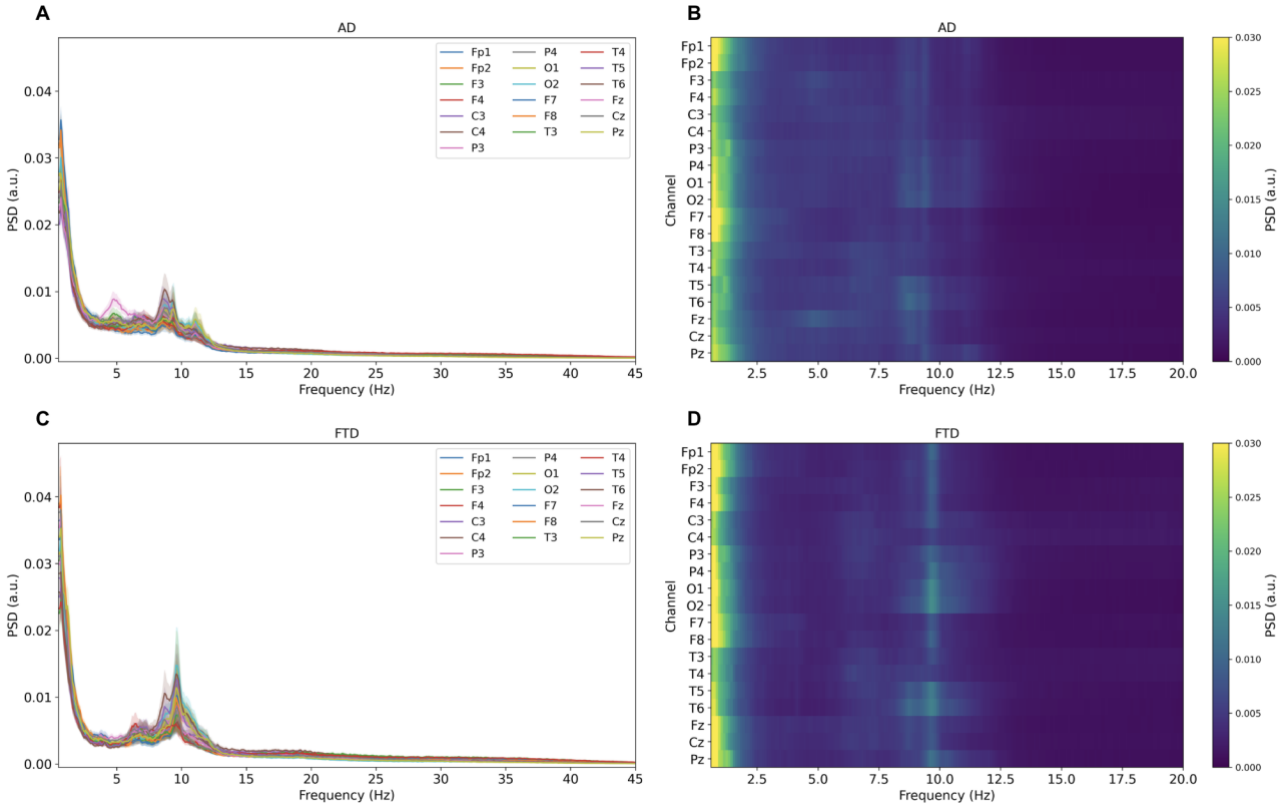

Fig. 11. Averaged Power Spectral Density for Alzheimer's Disease and Frontotemporal Dementia Groups: (A, C) Averaged PSD plots with shaded areas representing ± standard error of the mean (SEM), (B, D) Corresponding PSD heatmaps

Figure 12A illustrates the PSD that is averaged across channels for the group comparison. Overall, the most noticeable differences between AD and FTD appear in the low-frequency range (below ~14 Hz). In the delta band, the FTD group exhibits slightly higher power at the peak compared with the AD group. In the theta band, patients with AD show significantly higher ($p = 0.0312$) PSD values than FTD patients (Figure 12B). In the alpha band, the AD group has a tendency toward lower activity compared with the FTD, although this difference does not reach statistical significance ($p = 0.388$) (Figure 12C). No significant difference between the groups was observed when combining the theta and alpha PSD values ($p = 0.472$) (Figure 12D). At higher frequencies (>14 Hz), no activity is observed in either group. However, this absence of high-frequency activity is expected, as the EEG was recorded during resting state.

Currently, only a limited number of studies have identified spectral differences between AD and FTD. One study [75] reported findings consistent to this work, showing that AD patients exhibit increased theta power compared with FTD. However, evidence supporting such spectral differences remains limited, which highlights the need for further research to determine whether there is a consistent spectral differences between AD and FTD.

The results of the spectral analysis showed that differences in PSD values between AD and FTD were relatively small. For this reason, FC was selected for further analysis. Since the most noticeable group

differences were observed in the theta and alpha frequency ranges, only these two bands were selected for the FC analysis.

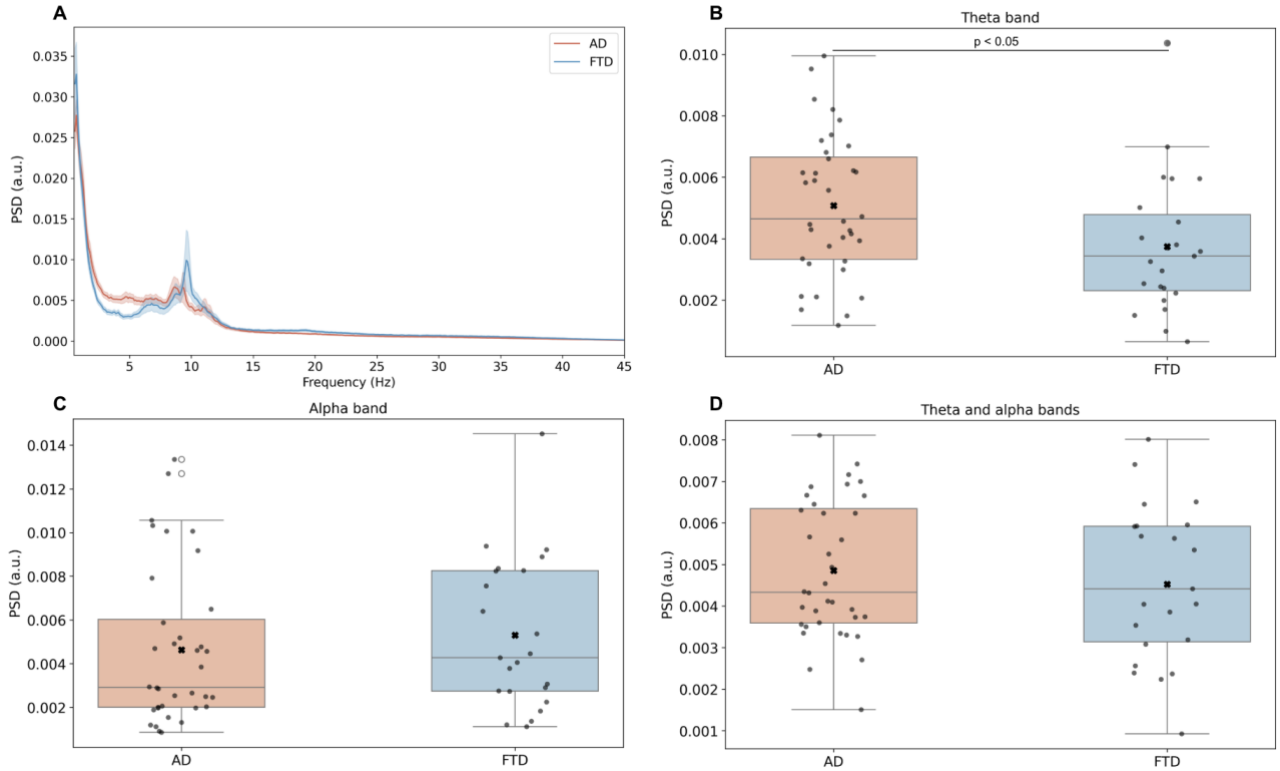

Fig. 12. Comparison of Averaged Power Spectral Density Between Alzheimer's Disease and Frontotemporal Dementia: (A) Full-spectrum averaged PSD with shaded areas representing ± standard error of the mean (SEM), (B) Comparison of theta band PSD values, (C) Comparison of alpha band PSD values, and (D) Comparison of combined theta-alpha PSD values

3.3. Functional connectivity analysis results

Pearson's correlation and coherence were calculated for the FC analysis. The group-averaged Pearson correlation matrices are shown in Figure 13. Although the AD and FTD matrices in both theta and alpha bands appear similar, the difference matrices (AD-FTD) reveal several distinct patterns.

In the theta band, the AD group exhibits stronger connectivity in the Fp1-F4 frontal connection, compared with the FTD. Overall, AD shows a tendency toward higher frontal connectivity with parietal (e.g. Fp1-P3, F4-P4, F3-Px), occipital (e.g. Fp1-O1, F3-O1), and posterior temporal (e.g. Fp2-T5, F3-T6) regions. Furthermore, AD demonstrates stronger connectivity between posterior temporal and parietal regions (e.g. T6-Pz, T6-P4) and between posterior temporal and occipital regions (e.g. T6-O1, T6-O2). Connectivity strengths in central and anterior temporal regions are similar between the groups. In conclusion, the most pronounced group differences are observed in frontal and posterior temporal connections, where the AD group shows stronger theta band connectivity.

The alpha band connectivity exhibits slightly different connectivity patterns. The AD group shows a tendency towards higher connectivity between frontal and parietal regions (e.g. Fp1-P3, Fp1-Pz), as well as slightly higher connectivity between frontal and temporal regions (e.g. Fp2-T5, Fp1-T5) compared with the FTD. Additionally, AD demonstrated relatively stronger connectivity across posterior cortical regions, involving posterior temporal, parietal and occipital areas (e.g. P3-P4, P3-

T5, O1-T5). In contrast, the FTD group tends to exhibit higher connectivity in central region (e.g. C3-Fz, C3-P4, Cz-F4), as well as in several frontal connections (e.g. Fp2-F7, F3-F4, F4-F7). Connectivity in other regions is similar between the groups or show a slight tendency towards higher connectivity in FTD group.

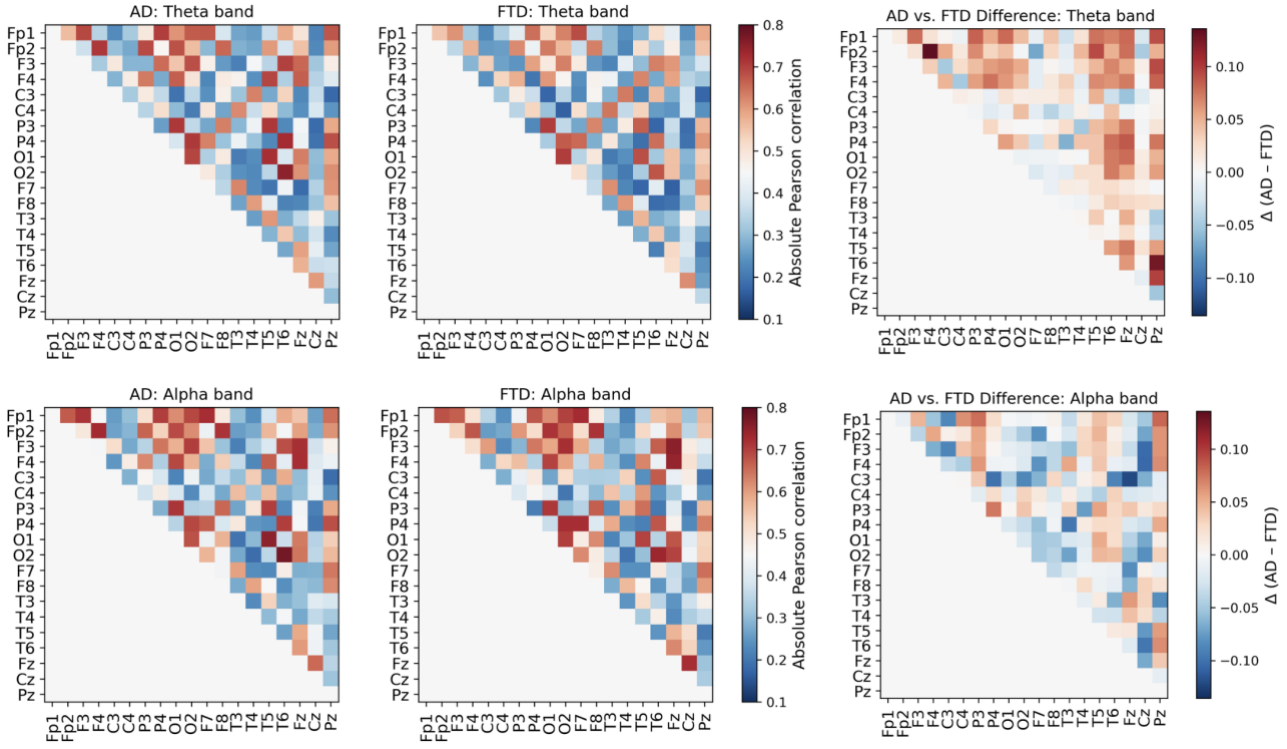

Fig. 13. Averaged Pearson Correlation Connectivity Matrices for Alzheimer's Disease and Frontotrmporal Dementia in Theta and Alpha Bands

The group-averaged coherence FC matrices are illustrated in Figure 14. The group-related connectivity patterns are mostly consistent to the Pearson correlation. In the theta band, the AD group shows a tendency toward increased connectivity in frontal and posterior temporal regions compared to the FTD. Connectivity in central and anterior temporal regions appear similar between the groups. In the alpha band, AD exhibits slightly stronger connectivity between frontal and temporal regions, between frontal and parietal regions, and across posterior cortical area. In contrast, FTD demonstrates a tendency toward increased connectivity in central and some frontal regions.

The observed differences in theta band FC, where the AD group shows stronger connectivity in frontal and posterior temporal regions compared to the FTD, may reflect the distinct patterns of neurodegeneration in these disorders. FTD mainly affects frontal and temporal cortical regions, while AD is associated with more widespread cortical impairment. Therefore, such differences in FC patterns between these diseases could be expected. However, to draw more reliable conclusions, it is essential to confirm these observations using statistical tests, which were not performed in this study. Therefore, further research is needed to determine whether FC patterns significantly differ between the AD and FTD groups.

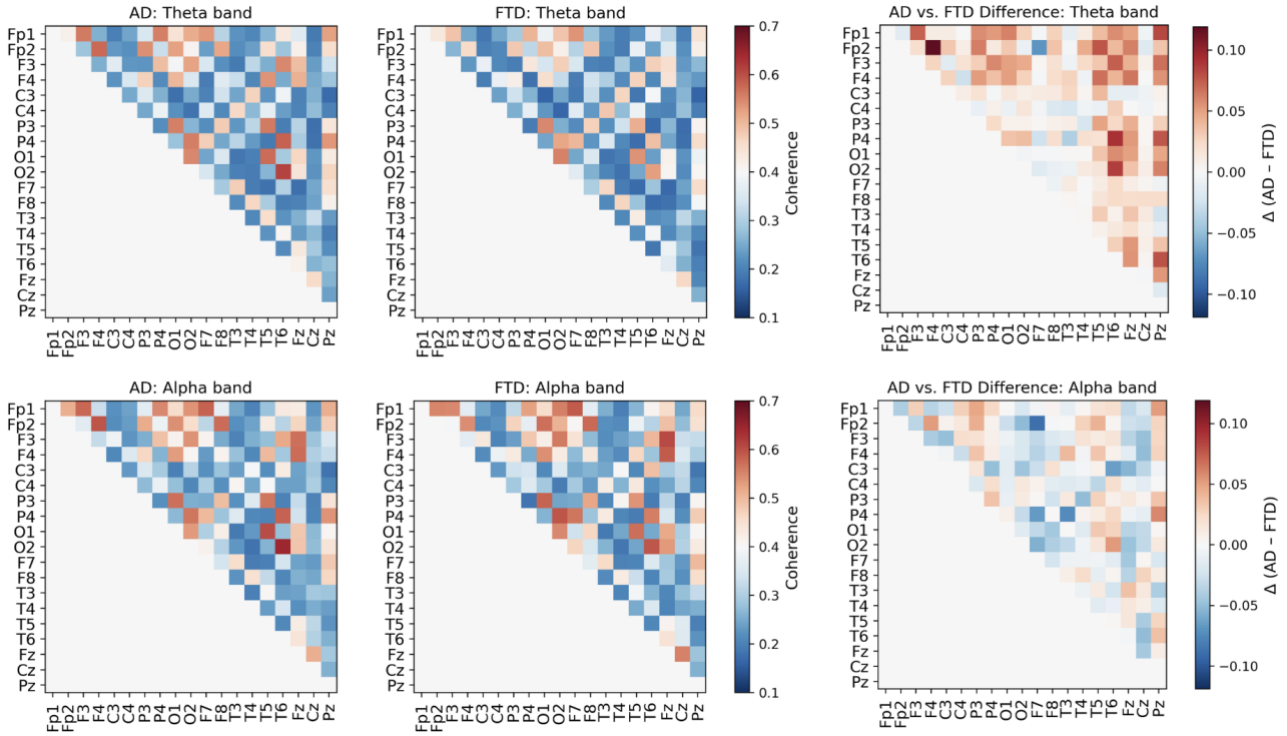

Fig. 14. Averaged Coherence Connectivity Matrices for Alzheimer's Disease and Frontotrmporal Dementia in Theta and Alpha Bands

The FC matrices were selected as input for the classification of AD and FTD because they provide detailed information about the connections between cortical regions, which could help to distinguish between these two diseases. Moreover, using connectivity features enables the identification of regional connections that contribute most strongly to the differentiation between AD and FTD.

3.4. Classification results

Since the input features prepared for the classification were matrices, a CNN was employed for the disease differentiation. Initially, an architecture search was conducted by experimenting with various numbers of convolutional layers, neurons per layer and hyperparameters. Each model was trained and evaluated five times, and the mean performance was used for model comparison. The results of all tested architectures are reported in Appendix 1 Table 4. Models with a single convolutional layer demonstrated accuracies ranging from 57.4 % to 61.8 %, while two-layer models achieved accuracies between 55.2% and 65.1%. Three-layer models showed accuracies ranging from 48.9% to 65.4%. The best two-layer model achieved similar results to the best three convolutional layer model. However, for further analysis, the model with the highest overall accuracy was selected. This model achieved an accuracy of 65.4% (SD = 1.4) and consisted of three convolutional layers with 64, 128, and 256 neurons, respectively, with kernel size of 3 × 3, batch normalization after each convolutional layer, followed by a flattening layer, dropout, and final layer with sigmoid activation function.

The selected CNN model was evaluated using LOSO cross-validation with multiple input configurations. These included Pearson correlation and coherence matrices computed in the theta or alpha frequency bands, which were used both separately and combined, as well as combined Pearson and coherence matrices. These input configurations were used to determine which frequency bands and connectivity measures provide the most informative features for distinguishing between AD and

FTD. For comparison, SVM classifier was evaluated using the same input sets. The classification results are summarised in Table 2.

The CNN-based classification achieved relatively similar performance across all input configurations. The lowest CNN performance was observed when using the alpha band coherence matrices, with an accuracy of 81.1% (SD = 31.3). The highest accuracies were achieved using the theta band coherence matrices (85.5%, SD = 25.5) and when combining Pearson correlation with coherence matrices in the theta band (85.6%, SD = 25.8). The SVM classifier demonstrated lower classification performance. The worst SVM results were achieved using the theta band Pearson correlation matrices, with an accuracy of 52.5% (SD = 36.1). While the best SVM performance was achieved using alpha band coherence matrices, with an accuracy of 57.1% (SD = 35.4). These results demonstrate that the proposed CNN model outperforms the SVM model across all tested input configurations for the AD and FTD classification.

Table 2. The Performance of Alzheimer's Disease and Frontotemporal Dementia Classification Using EEG Functional Connectivity Features. Values represent mean accuracy ± SD obtained using LOSO cross-validation

	Method	**Theta + Alpha**	**Theta**	**Alpha**
Pearson correlation	CNN	84.2 ± 30.5	83.5 ± 29.5	84.3 ± 26.9
	SVM	55.8 ± 38.5	52.5 ± 36.1	55.9 ± 37.8
Coherence	CNN	83.4 ± 30.1	85.5 ± 25.5	81.1 ± 31.3
	SVM	56.9 ± 36.7	53.4 ± 35.9	57.1 ± 35.4
Pearson correlation + coherence	CNN	84.6 ± 29.4	**85.6 ± 25.8**	83.8 ± 29.0
	SVM	55.9 ± 37.9	53.3 ± 36.1	56.5 ± 37.9

Figure 15 demonstrates the confusion matrices obtained from the CNN-based classification. Across all evaluated input configurations, the number of correctly classified individuals with AD ranged from 28 to 33, while the number of correctly classified individuals with FTD ranged from 20 to 21. These results show that, in most cases, a higher number of misclassifications occurred for AD subjects compared with FTD.

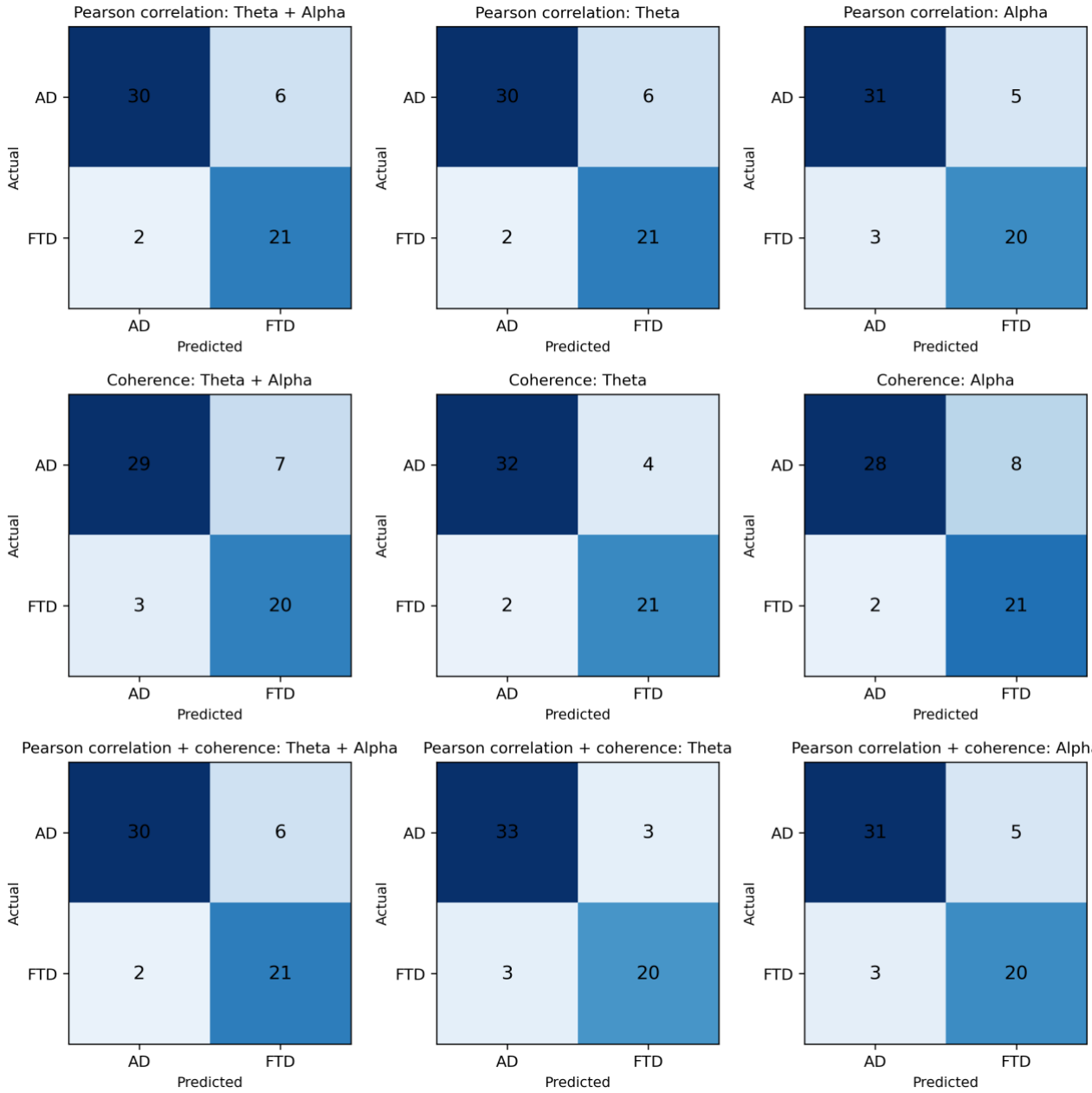

Fig. 15. Subject-Level Confusion Matrices for CNN-Based Classification of Alzheimer's Disease and Frontotemporal Dementia Using EEG Functional Connectivity Features

These CNN-based classification results raise concern about the robustness of the model's performance. Firstly, because there is a considerable difference between the results obtained during the CNN architecture search using a subject-wise 70/15/15 train-validation-test split and those obtained utilising LOSO cross-validation with the same input features. The subject-wise split achieved a lower accuracy of 65.4%, while LOSO validation resulted in higher mean accuracy of 84.2%. However, the LOSO results exhibited a large standard deviation. The train-validation-test split had lower accuracy, likely due to the smaller number of subjects available for training, but provided a more stable model performance. In contrast, LOSO validation enabled the model to be trained on a larger number of subjects, which resulted in higher average accuracy, but also increased variability.

Therefore, additional analysis was conducted to investigate the possible reasons for this increased variability. Figure 16 presents the classification accuracy obtained in each LOSO iteration. These results show that the model achieved high performance for some subjects but low performance for others. For example, for Subjects 4, 12, and 13, the model demonstrated near-zero accuracy across the majority of input configurations. For other subjects, accuracy values varied across input sets and seemed to be distributed randomly, as observed for Subjects 8, 29, and 48. In contrast, several subjects (e.g. Subjects 1, 2, 10, 21, and 52) achieved consistently high classification accuracy across all tested input configurations. Interestingly, no consistent pattern is observed indicating that a particular feature set led to lower accuracy.

These results suggest that some subjects share similar feature patterns, which enables the model to learn and accurately classify those subjects. Meanwhile, subjects whose features deviate from these learned patterns are more likely to be misclassified or inconsistently assigned to a class. In conclusion, this indicates that the model has not learned stable features that generalise well across most subjects, but instead it relies on subject-specific patterns that perform well for certain individuals but fail for others.

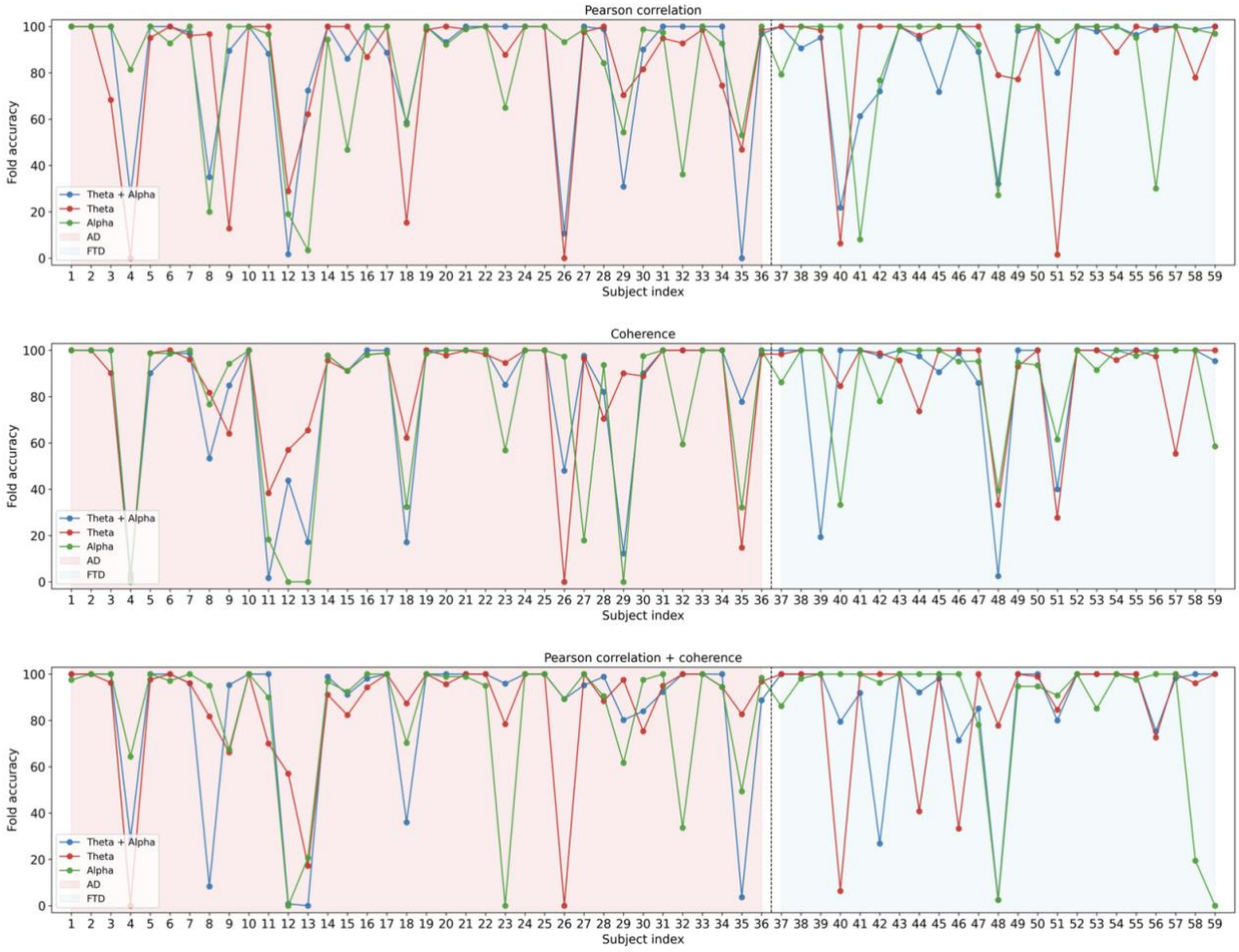

Fig. 16. Classification Accuracy Obtained Using Leave-One-Subject-Out Validation for CNN-based classification of Alzheimer's Disease and Frontotemporal Dementia: Each point corresponds to the classification accuracy for a single left-out subject.

To further investigate this classification performance, several subject-level epoch-averaged FC matrices were analysed. Two AD individuals that were always classified correctly (Subjects 1 and 2) and two AD subjects that were mostly misclassified (Subject 4 and 12), were selected for this analysis. The epoch-averaged Pearson correlation connectivity matrices are presented in Figure 17. Additionally, Pearson correlation coefficients were computed to quantify the similarity between connectivity matrices of these subjects. The results are summarised in Table 3.

A visual comparison of the matrices indicate that Subject 12 exhibits lower theta band connectivity across the majority of channel pairs compared with Subjects 1 and 2. Previous group level FC comparison showed that the FTD group tends to exhibit weaker frontal and temporal region connectivity compared with the AD. Therefore, reduced Subject 12 connectivity could be a contributing factor to the frequent misclassification of this subject. The connectivity matrices appeared visually similar, without any clear differences, in the remaining subjects and frequency bands.

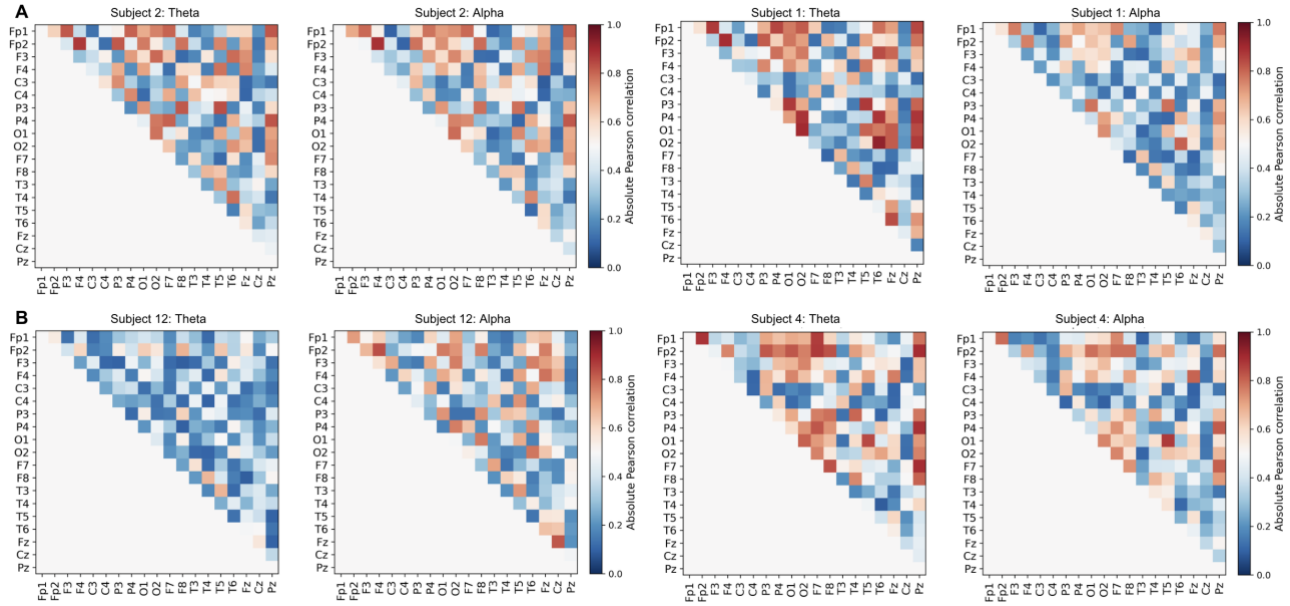

Fig. 17. Epoch-Averaged Pearson Correlation Functional Connectivity Matrices for Selected Alzheimer's Disease Subjects: (A) Subjects consistently classified correctly by the CNN model, (B) Subjects mostly misclassified by the CNN model

The Pearson correlation coefficient between the theta band matrices of two correctly classified subjects (Subjects 1 and 2) was relatively high (r = 0.757), with stronger similarity observed in the alpha band matrices (r = 0.852). In contrast, the correlation between the two consistently misclassified subjects (Subjects 4 and 12) was considerably lower, both in the theta band (r = 0.372) and the alpha band (r = 0.313). The correlation between subjects classified correctly and incorrectly was found to be generally lower than that observed between Subjects 1 and 2. For example, Subject 2 exhibited correlations of 0.626 (theta) and 0.510 (alpha) with Subject 12, and 0.519 (theta) and 0.671 (alpha) with Subject 4. Similarly, Subject 1 demonstrated correlations of 0.521 (theta) and 0.565 (alpha) with Subject 12, and 0.499 (theta) and 0.626 (alpha) with Subject 4.

From these results, it is visible that Subject 4 showed relatively higher alpha band correlation with Subject 2 compared with other subject pairs. However, Subject 4 was correctly classified in two out

of nine tested input configurations, both of which involved the alpha band Pearson correlation features (see Figure 16).

These findings suggest that the CNN model tends to classify subjects more accurately when their connectivity patterns are similar to those subjects learned during training, while subjects with more distinct connectivity patterns are more likely to be misclassified. This supports the earlier hypothesis that the model might rely on subject-specific patterns rather than features that generalise well across all individuals. However, to draw more reliable conclusions, a more detailed analysis involving similarity assessment across all subjects and connectivity measures is needed.

Table 3. Pearson Correlation-Based Similarity Between Functional Connectivity Matrices of Selected Subject Pairs in the Theta and Alpha bands

Subject pair	**Pearson correlation (Theta)**	**Pearson correlation (Alpha)**
Subject 1 – Subject 2	0.757	0.852
Subject 12 – Subject 4	0.372	0.313
Subject 2 – Subject 12	0.626	0.510
Subject 2 – Subject 4	0.519	0.671
Subject 1 – Subject 12	0.521	0.565
Subject 1 – Subject 4	0.449	0.626

In conclusion, the classification accuracy achieved in this work is consistent with results reported in previous studies that employed LOO or LOSO validations. In this study proposed CNN-based method achieved an accuracy of 85.6% (SD = 25.8). For comparison, study [54] reported an accuracy of 73% (SD = 11) for the classification of AD and FTD using a decision tree model. Study [76] achieved an accuracy of 72.88% with SVM classifier, although no measure of variability was reported. Another study [56] utilising SVM-based method reported an accuracy of 96.6% but also did not provide the value of standard deviation. The accuracy obtained in this study exceeds the AD and FTD classification results in several previous studies. However, the direct comparison across studies is challenging due to the frequent absence of reported variability measures.

3.5. Feature importance results

To identify which channel pairs contributed most strongly to the CNN-based classification, Gradient ⊙ Input saliency method was employed. This method was selected because it provides fast local explanation of model predictions and it is computationally efficient [77]. The resulting feature importance maps are presented in Figure 18. Across most input configurations, the Fp1-F4 connection was identified as the most important feature. This channel pair is displayed in blue, indicating its contribution to the AD class (where AD = 0 and FTD = 1). Therefore, a reduction in the connectivity strength of this feature reduces the model's confidence in predicting AD. Furthermore, with the alpha band Pearson correlation input set, the Fp1-F8 connection showed higher importance. When using the theta band as input, the O1-O2 connection was identified as an important feature contributing to FTD. In contrast, when using only the alpha band as input, the importance of O1-O2 connection decreased and other connections, such as P4-F7 and Fp2-F7, became more important. Additionally, for the alpha band input, the O2-T6 connection appears among the most important features. To summarise, the most important features were found to be located in frontal and occipital cortical connections.

As discussed previously, frontal connectivity patterns differ between the AD and FTD, which may explain why frontal connections play an important role in distinguishing these disorders. In contrast, no clear differences in occipital region were observed when comparing the AD and FTD connectivity matrices. However, study [56] also identified the O1-O2 connection as one of the most important features, suggesting that occipital connectivity may play a role in differentiating AD and FTD. However, these findings should be interpreted carefully, as only a few studies have investigated this and supporting evidence remains limited. Understanding which specific regional connections influence classification decisions may provide valuable insights that could help to improve the differentiation between AD and FTD. Therefore, further research is needed to confirm and extend these connectivity feature importance findings.

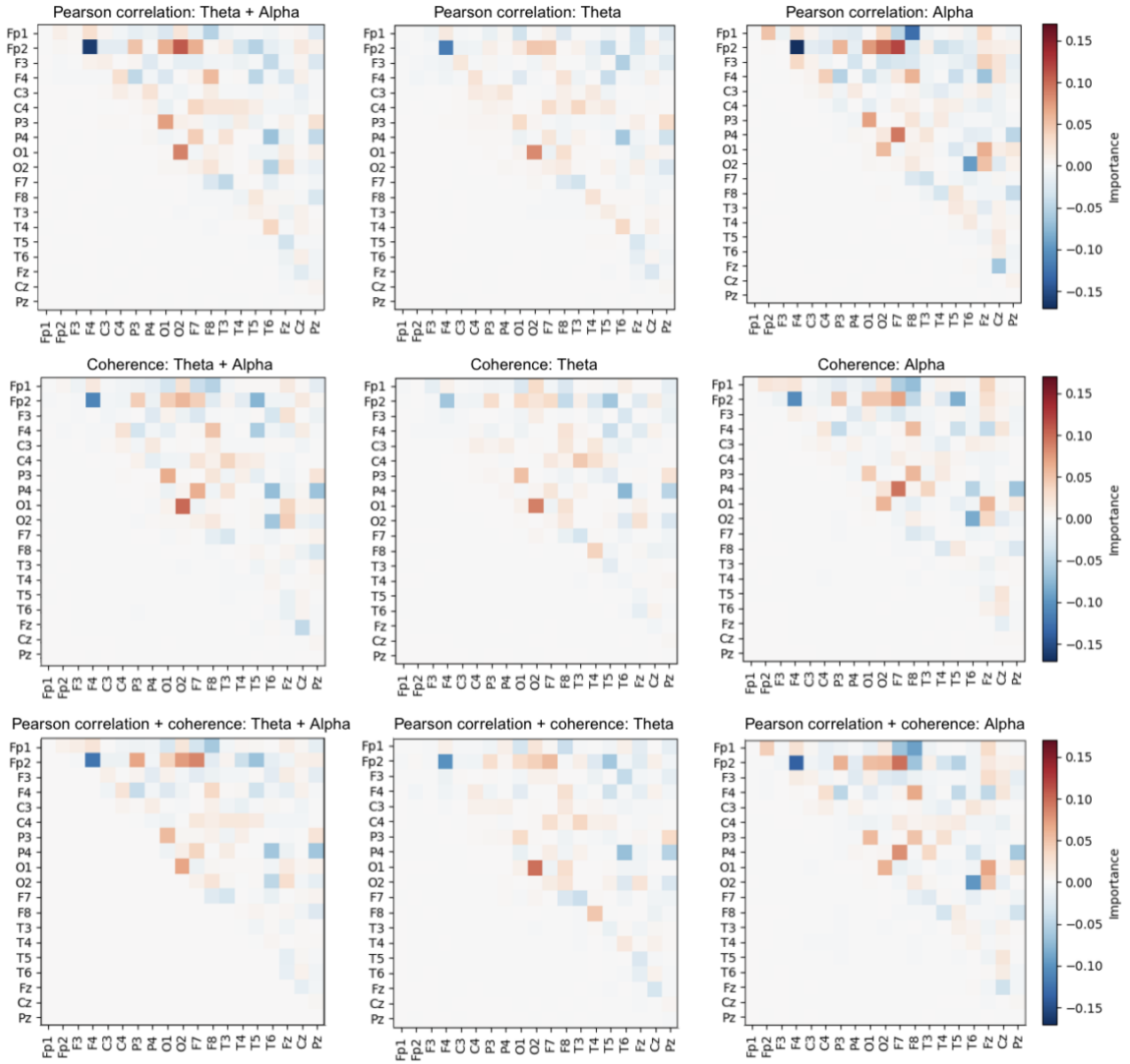

Fig. 18. Averaged Gradient ⊙ Input Saliency Maps Showing Important EEG Connectivity Features for CNN-based Classification of Alzheimer's Disease and Frontotemporal Dementia

3.6. Limitations and future perspectives

This project has several limitations. Firstly, the data used in this study did not provide information about the FTD patients subtypes (bvFTD, svPPA and nfvPPA). Additionally, the group sizes were slightly imbalanced, which may have affected the classification performance. Another important limitation is the small sample size. The use of larger dataset would allow for more reliable and generalisable results. Furthermore, the EEG recordings utilised in this work were collected using only 19 electrodes, however higher-density EEG recordings could provide improved spatial resolution and more detailed connectivity information. Therefore, future studies could investigate how the proposed model performs on datasets with a larger number of EEG channels. Due to time limitations, the CNN architecture search was conducted using only a single input configuration. However, different connectivity features may perform better with other architectures. Therefore, a more detailed architecture search using different input sets could be beneficial. Finally, the model was not evaluated using different datasets. Therefore, future research could validate the proposed model using additional datasets to better assess its performance and reliability.

Conclusions

1. Individuals diagnosed with Alzheimer's disease exhibited significantly higher theta band (4–8 Hz) power than patients with frontotemporal dementia, with no significant differences found in other frequency bands.
2. Compared with frontotemporal dementia, the Alzheimer's disease group showed a tendency toward stronger theta band connectivity in frontal and posterior temporal regions. Frontotemporal dementia exhibited a tendency toward stronger alpha band connectivity in central regions compared with Alzheimer's disease.
3. The CNN architecture search revealed that a three-layer model with batch normalisation and dropout achieved the best performance among all tested configurations.
4. All input feature sets had a similar impact on the final performance of the machine learning models. In the classification of Alzheimer's disease and frontotemporal dementia, the CNN-based model achieved higher performance, with a maximum accuracy of 85.6% (SD = 25.8), compared with the SVM classifier, with a maximum accuracy of 57.1% (SD = 35.4).
5. The most important connectivity features for distinguishing Alzheimer's disease and frontotemporal dementia were observed in frontal and occipital region connections.

List of references

1. HARRISON DENING, Karen. and BURNS, Alistair S. Evidence-based practice in dementia for nurses and nursing students. *Jessica Kingsley Publishers*, 2019. p. 12–26. ISBN 9781784507978.
2. KARANTZOULIS, Stella and GALVIN, James E. Distinguishing Alzheimer's disease from other major forms of dementia. *Expert Review of Neurotherapeutics*. 9 November 2011. Vol. 11, no. 11, p. 1579–1591. DOI 10.1586/ern.11.155.
3. KAYE, Jeffrey A. Diagnostic challenges in dementia. *Neurology*. July 1998. Vol. 51, no. 1_suppl_1. DOI 10.1212/WNL.51.1_Suppl_1.S45.
4. EMMADY, Prabhu D., et al. Major Neurocognitive Disorder (Dementia) (Nursing). *StatPearls*, 2022. Available from: https://www.ncbi.nlm.nih.gov/books/NBK570552/
5. ARVANITAKIS, Zoe, et al. Diagnosis and Management of Dementia: Review. *JAMA*. 22 October 2019. Vol. 322, no. 16, p. 1589. DOI 10.1001/jama.2019.4782.
6. STEFANOU, Konstantinos, et al. A Novel CNN-Based Framework for Alzheimer's Disease Detection Using EEG Spectrogram Representations. *Journal of Personalized Medicine*. 14 January 2025. Vol. 15, no. 1, p. 27. DOI 10.3390/jpm15010027.
7. SCHELTENS, Philip, et al. Alzheimer's disease. *The Lancet*. April 2021. Vol. 397, no. 10284, p. 1577–1590. DOI 10.1016/S0140-6736(20)32205-4.
8. KAMATHAM, et al. Pathogenesis, diagnostics, and therapeutics for Alzheimer's disease: Breaking the memory barrier. *Ageing Research Reviews*. November 2024. Vol. 101, p. 102481. DOI 10.1016/j.arr.2024.102481.
9. KUMAR THAKUR, Ajit, et al. Pathophysiology and management of alzheimer's disease: an overview. *Journal of Analytical & Pharmaceutical Research*. 26 April 2018. Vol. 7, no. 2. DOI 10.15406/japlr.2018.07.00230.
10. BREIJYEH, Zeinab and KARAMAN, Rafik. Comprehensive Review on Alzheimer's Disease: Causes and Treatment. *Molecules*. 8 December 2020. Vol. 25, no. 24, p. 5789. DOI 10.3390/molecules25245789.
11. THAL, Dietmar R., et al. Phases of Aβ-deposition in the human brain and its relevance for the development of AD. *Neurology*. 25 June 2002. Vol. 58, no. 12, p. 1791–1800. DOI 10.1212/WNL.58.12.1791.
12. ABUBAKAR, Murtala Bello, et al. Alzheimer's Disease: An Update and Insights Into Pathophysiology. *Frontiers in Aging Neuroscience*. 30 March 2022. Vol. 14. DOI 10.3389/fnagi.2022.742408.
13. BRAAK, H. and BRAAK, E. Neuropathological stageing of Alzheimer-related changes. *Acta Neuropathologica*. September 1991. Vol. 82, no. 4, p. 239–259. DOI 10.1007/BF00308809.
14. CHÉTELAT, Gaël, et al. Amyloid-PET and 18F-FDG-PET in the diagnostic investigation of Alzheimer's disease and other dementias. *The Lancet Neurology*. November 2020. Vol. 19, no. 11, p. 951–962. DOI 10.1016/S1474-4422(20)30314-8.
15. HAASS, Christian and SELKOE, Dennis J. Soluble protein oligomers in neurodegeneration: lessons from the Alzheimer's amyloid β-peptide. *Nature Reviews Molecular Cell Biology*. February 2007. Vol. 8, no. 2, p. 101–112. DOI 10.1038/nrm2101.
16. CLINE, Erika N., et al. The Amyloid-β Oligomer Hypothesis: Beginning of the Third Decade. *Journal of Alzheimer's Disease*. 12 June 2018. Vol. 64, no. s1, p. S567–S610. DOI 10.3233/JAD-179941.

17. PASSERI, Elodie, et al. Alzheimer's Disease: Treatment Strategies and Their Limitations. *International Journal of Molecular Sciences*. 12 November 2022. Vol. 23, no. 22, p. 13954. DOI 10.3390/ijms232213954.
18. SPOCTER, Muhammad A., et al. Neuropil distribution in the cerebral cortex differs between humans and chimpanzees. *Journal of Comparative Neurology*. 7 September 2012. Vol. 520, no. 13, p. 2917–2929. DOI 10.1002/cne.23074.
19. MUCKE, Lennart. Alzheimer's disease. *Nature*. 14 October 2009. Vol. 461, no. 7266, p. 895–897. DOI 10.1038/461895a.
20. SPIRES-JONES, Tara L. and HYMAN, Bradley T. The Intersection of Amyloid Beta and Tau at Synapses in Alzheimer's Disease. *Neuron*. May 2014. Vol. 82, no. 4, p. 756–771. DOI 10.1016/j.neuron.2014.05.004.
21. SZABLEWSKI, Leszek. Glucose Transporters in Brain: In Health and in Alzheimer's Disease. *Journal of Alzheimer's Disease*. 20 December 2016. Vol. 55, no. 4, p. 1307–1320. DOI 10.3233/JAD-160841.
22. SIMPSON, Ian A., et al. Decreased concentrations of GLUT1 and GLUT3 glucose transporters in the brains of patients with Alzheimer's disease. *Annals of Neurology*. 8 May 1994. Vol. 35, no. 5, p. 546–551. DOI 10.1002/ana.410350507.
23. RAUT, Snehal, et al. Hypometabolism, Alzheimer's Disease, and Possible Therapeutic Targets: An Overview. *Cells*. 8 August 2023. Vol. 12, no. 16, p. 2019. DOI 10.3390/cells12162019.
24. PORSTEINSSON, A.P., et al. Diagnosis of Early Alzheimer's Disease: Clinical Practice in 2021. *The Journal of Prevention of Alzheimer's Disease*. July 2021. Vol. 8, no. 3, p. 371–386. DOI 10.14283/jpad.2021.23.
25. CUMMINGS, Jeffrey. The Role of Biomarkers in Alzheimer's Disease Drug Development. *Advances in experimental medicine and biology*. 2019. Vol. 1118, p. 29–61. DOI 10.1007/978-3-030-05542-4_2.
26. JACK, Clifford R., et al. NIA-AA Research Framework: Toward a biological definition of Alzheimer's disease. *Alzheimer's & Dementia*. April 2018. Vol. 14, no. 4, p. 535–562. DOI 10.1016/j.jalz.2018.02.018.
27. PUPPALA, Goutham Kumar, et al. Frontotemporal Dementia – Current Concepts. *Neurology India*. September 2021. Vol. 69, no. 5, p. 1144–1152. DOI 10.4103/0028-3886.329593.
28. ANTONIONI, Annibale, et al. Frontotemporal Dementia, Where Do We Stand? A Narrative Review. *International Journal of Molecular Sciences*. 21 July 2023. Vol. 24, no. 14, p. 11732. DOI 10.3390/ijms241411732.
29. PEET, Bradley T., et al. Neuroimaging in Frontotemporal Dementia: Heterogeneity and Relationships with Underlying Neuropathology. *Neurotherapeutics*. April 2021. Vol. 18, no. 2, p. 728–752. DOI 10.1007/s13311-021-01101-x.
30. GORNO-TEMPINI, M.L., et al. Classification of primary progressive aphasia and its variants. *Neurology*. 15 March 2011. Vol. 76, no. 11, p. 1006–1014. DOI 10.1212/WNL.0b013e31821103e6.
31. TIPPETT, Donna C and KESER, Zafer. Clinical and neuroimaging characteristics of primary progressive aphasia. *Handbook of clinical neurology*. 2022. Vol. 185, p. 81–97. DOI 10.1016/B978-0-12-823384-9.00016-5.
32. BAHIA, Valéria Santoro, et al. Neuropathology of frontotemporal lobar degeneration: A review. *Dementia & Neuropsychologia*. March 2013. Vol. 7, no. 1, p. 19–26. DOI 10.1590/S1980-57642013DN70100004.

33. BORGHESANI, Valentina, et al. Frontotemporal dementia: A unique window on the functional role of the temporal lobes. *Handbook of clinical neurology*. 2022. Vol. 187, p. 429–448. DOI 10.1016/B978-0-12-823493-8.00011-0.
34. XIAO, Die, LI, Jianyu, et al. Association of cortical morphology, white matter hyperintensity, and glymphatic function in frontotemporal dementia variants. *Alzheimer's & Dementia*. 11 September 2024. Vol. 20, no. 9, p. 6045–6059. DOI 10.1002/alz.14158.
35. BOEVE, Bradley F. Behavioral Variant Frontotemporal Dementia. *Continuum*. June 2022. Vol. 28, no. 3, p. 702–725. DOI 10.1212/CON.0000000000001105.
36. NEYLAN, Kyra D. and MILLER, Bruce L. New Approaches to the Treatment of Frontotemporal Dementia. *Neurotherapeutics*. July 2023. Vol. 20, no. 4, p. 1055–1065. DOI 10.1007/s13311-023-01380-6.
37. CHU, Andrew and WADHWA, Roopma. Selective Serotonin Reuptake Inhibitors. *StatPearls*. 2023. Available from: https://www.ncbi.nlm.nih.gov/books/NBK554406/
38. GOSSYE, Helena, et al. The Use of Biomarkers and Genetic Screening to Diagnose Frontotemporal Dementia: Evidence and Clinical Implications. *Frontiers in Neuroscience*. 6 August 2019. Vol. 13. DOI 10.3389/fnins.2019.00757.
39. SOUZA, Leonardo Cruz de, et al. Diagnosis of frontotemporal dementia: recommendations of the Scientific Department of Cognitive Neurology and Aging of the Brazilian Academy of Neurology. *Dementia & Neuropsychologia*. September 2022. Vol. 16, no. 3 suppl 1, p. 40–52. DOI 10.1590/1980-5764-dn-2022-s103pt.
40. TAKADA, Leonel T. The Genetics of Monogenic Frontotemporal Dementia. *Dementia & Neuropsychologia*. September 2015. Vol. 9, no. 3, p. 219–229. DOI 10.1590/1980-57642015dn93000003.
41. BIASIUCCI, Andrea, et al. Electroencephalography. *Current Biology*. February 2019. Vol. 29, no. 3, p. R80–R85. DOI 10.1016/j.cub.2018.11.052.
42. TEPLAN, M. Fundamentals of EEG Measurement. *Measurement Science Review*. 2002. Vol. 2. Available from: https://www.measurement.sk/2002/S2/Teplan.pdf
43. DAMBORSKÁ, Alena, et al. EEG Resting-State Large-Scale Brain Network Dynamics Are Related to Depressive Symptoms. *Frontiers in Psychiatry*. 9 August 2019. Vol. 10. DOI 10.3389/fpsyt.2019.00548.
44. SOLOMON, Jr, O M. PSD computations using Welch's method. [Power Spectral Density (PSD)]. 1991. DOI 10.2172/5688766.
45. COCHRAN, W., et al. What is the fast Fourier transform? *IEEE Transactions on Audio and Electroacoustics*. June 1967. Vol. 15, no. 2, p. 45–55. DOI 10.1109/TAU.1967.1161899.
46. PEREZ, Vanesa, et al. EEG frequency bands in subjective cognitive decline: A systematic review of resting state studies. *Biological Psychology*. September 2024. Vol. 191, p. 108823. DOI 10.1016/j.biopsycho.2024.108823.
47. ZHANG, Haifeng, et al. The Significance of EEG Alpha Oscillation Spectral Power and Beta Oscillation Phase Synchronization for Diagnosing Probable Alzheimer Disease. *Frontiers in Aging Neuroscience*. 7 June 2021. Vol. 13. DOI 10.3389/fnagi.2021.631587.
48. TIWARI, Smita, et al. MIDNN- a classification approach for the EEG based motor imagery tasks using deep neural network. *Applied Intelligence*. 29 March 2022. Vol. 52, no. 5, p. 4824–4843. DOI 10.1007/s10489-021-02622-w.
49. WU, Shijing, et al. Changes of brain functional network in Alzheimer's disease and frontotemporal dementia: a graph-theoretic analysis. *BMC Neuroscience*. 4 July 2024. Vol. 25, no. 1, p. 30. DOI 10.1186/s12868-024-00877-w.

50. BRIELS, Casper T., et al. Reproducibility of EEG functional connectivity in Alzheimer's disease. *Alzheimer's Research & Therapy*. 3 December 2020. Vol. 12, no. 1, p. 68. DOI 10.1186/s13195-020-00632-3.
51. MILTIADOUS, Andreas, et al. Machine Learning Algorithms for Epilepsy Detection Based on Published EEG Databases: A Systematic Review. *IEEE Access*. 2023. Vol. 11, p. 564–594. DOI 10.1109/ACCESS.2022.3232563.
52. GERAEDTS, Victor J., et al. Clinical correlates of quantitative EEG in Parkinson disease. *Neurology*. 6 November 2018. Vol. 91, no. 19, p. 871–883. DOI 10.1212/WNL.0000000000006473.
53. AKBARI, Hesam, et al. Classification of normal and depressed EEG signals based on centered correntropy of rhythms in empirical wavelet transform domain. *Health Information Science and Systems*. 6 December 2021. Vol. 9, no. 1, p. 9. DOI 10.1007/s13755-021-00139-7.
54. MILTIADOUS, Andreas, et al. Alzheimer's Disease and Frontotemporal Dementia: A Robust Classification Method of EEG Signals and a Comparison of Validation Methods. *Diagnostics*. 9 August 2021. Vol. 11, no. 8, p. 1437. DOI 10.3390/diagnostics11081437.
55. ZHENG, Huang, et al. Time-Frequency functional connectivity alterations in Alzheimer's disease and frontotemporal dementia: An EEG analysis using machine learning. *Clinical Neurophysiology*. February 2025. Vol. 170, p. 110–119. DOI 10.1016/j.clinph.2024.12.008.
56. MA, Yuan, et al. Classification of Alzheimer's Disease and Frontotemporal Dementia Using Electroencephalography to Quantify Communication between Electrode Pairs. *Diagnostics*. 30 September 2024. Vol. 14, no. 19, p. 2189. DOI 10.3390/diagnostics14192189.
57. MILTIADOUS, Andreas, et al. A Dataset of Scalp EEG Recordings of Alzheimer's Disease, Frontotemporal Dementia and Healthy Subjects from Routine EEG. *Data*. 27 May 2023. Vol. 8, no. 6, p. 95. DOI 10.3390/data8060095.
58. KIM, Do-Won and IM, Chang-Hwan. EEG Spectral Analysis. *Springer*. 2018. p. 35–53. DOI 10.1007/978-981-13-0908-3_3.
59. MILJEVIC, Aleksandra, et al. Alterations in EEG functional connectivity in individuals with depression: A systematic review. *Journal of Affective Disorders*. 1 May 2023. Vol. 328, p. 287–302. DOI 10.1016/j.jad.2023.01.126
60. SAKIB, Shadman, et al. An Overview of Convolutional Neural Network: Its Architecture and Applications. *Preprints*. 20 November 2018. DOI 10.20944/preprints201811.0546.v1.
61. GHOLAMIANGONABADI, Davoud, et al. Deep Neural Networks for Human Activity Recognition With Wearable Sensors: Leave-One-Subject-Out Cross-Validation for Model Selection. *IEEE Access*. 2020. Vol. 8, p. 133982–133994. DOI 10.1109/ACCESS.2020.3010715.
62. SIMONYAN, Karen, et al. Deep Inside Convolutional Networks: Visualising Image Classification Models and Saliency Maps. 19 April 2014. DOI 10.48550/arXiv.1312.6034.
63. SHRIKUMAR, Avanti, et al. Learning Important Features Through Propagating Activation Differences. *PMLR*. 12 October 2019. p. 3245–3153. DOI 10.48550/arXiv.1704.02685.
64. ADEBAYO, Julius, et al. Sanity Checks for Saliency Maps. *Neural Information Processing Systems*. 6 November 2020. DOI 10.48550/arXiv.1810.03292.
65. GRAMFORT, Alexandre. MEG and EEG data analysis with MNE-Python. *Frontiers in Neuroscience*. 2013. Vol. 7. DOI 10.3389/fnins.2013.00267.
66. VIRTANEN, Pauli, et al. SciPy 1.0: fundamental algorithms for scientific computing in Python. *Nature Methods*. 2 March 2020. Vol. 17, no. 3, p. 261–272. DOI 10.1038/s41592-019-0686-2.
67. ABADI, Martín, et al. TensorFlow: Large-Scale Machine Learning on Heterogeneous Distributed Systems. 16 March 2016. DOI 10.48550/arXiv.1603.04467.

68. PEDREGOSA, Fabian, et al. Scikit-learn: Machine Learning in Python. *Journal of Machine Learning Research*. 5 June 2018. DOI 10.48550/arXiv.1201.0490
69. VAN ROSSUM, Guido and DRAKE, Fred. L. Python 3 Reference Manual. 2009.
70. HARRIS, Charles R., et al. Array programming with NumPy. *Nature*. 17 September 2020. Vol. 585, no. 7825, p. 357–362. DOI 10.1038/s41586-020-2649-2.
71. MCKINNEY, Wes. Data Structures for Statistical Computing in Python. 2010. p. 56–61. DOI 10.25080/Majora-92bf1922-00a.
72. HUNTER, John D. Matplotlib: A 2D Graphics Environment. *Computing in Science & Engineering*. 2007. Vol. 9, no. 3, p. 90–95. DOI 10.1109/MCSE.2007.55.
73. WASKOM, Michael. seaborn: statistical data visualization. *Journal of Open Source Software*. 6 April 2021. Vol. 6, no. 60, p. 3021. DOI 10.21105/joss.03021.
74. KURLOWICZ, Lenore and WALLACE, Meredith. The Mini Mental State Examination (MMSE) Online. 1999. Available from: www.hartfordign.org.
75. CASO, Francesca, et al. Quantitative EEG and LORETA: valuable tools in discerning FTD from AD? *Neurobiology of Aging*. October 2012. Vol. 33, no. 10, p. 2343–2356. DOI 10.1016/j.neurobiolaging.2011.12.011.
76. ZHENG, Huang, et al. Multi-Threshold Recurrence Rate Plot: A Novel Methodology for EEG Analysis in Alzheimer's Disease and Frontotemporal Dementia. *Brain Sciences*. 1 June 2024. Vol. 14, no. 6, p. 565. DOI 10.3390/brainsci14060565.
77. ANCONA, Marco, et al. Towards better understanding of gradient-based attribution methods for Deep Neural Networks. *International Conference on Learning Representations*. 16 November 2017. DOI 10.48550/arXiv.1711.06104

Appendices

Appendix 1. CNN architecture search results

Table 4. The Performance of CNN Architectures Evaluated During an Architecture Search

Model archirecture	**Mean ± std accuracy**
Learning rate: 0.001; Batch size: 16	
Conv2D(8, 2x2) → Flatten → Dropout(0.4) → Dense(1, sigmoid)	60.2 ± 1.9
Conv2D(16, 2x2) → Flatten → Dropout(0.4) → Dense(1, sigmoid)	60.9 ± 1.8
Conv2D(32, 2x2) → Flatten → Dropout(0.4) → Dense(1, sigmoid)	60.8 ± 2.4
Conv2D(64, 2x2) → Flatten → Dropout(0.4) → Dense(1, sigmoid)	61.8 ± 1.2
Conv2D(128, 2x2) → Flatten → Dropout(0.4) → Dense(1, sigmoid)	60.8 ± 2.0
Conv2D(64, 2x2) → BachNorm → Flatten → Dropout(0.4) → Dense(1, sigmoid)	58.3 ± 1.5
Conv2D(64, 2x2) → MaxPooling(2x2) → Flatten → Dropout(0.4) → Dense(1, sigmoid)	58.8 ± 0.6
Conv2D(64, 2x2) → BachNorm → MaxPooling(2x2) → Flatten → Dropout(0.4) → Dense(1, sigmoid)	57.4 ± 0.4
Conv2D(64, 3x3) → Flatten → Dropout(0.4) → Dense(1, sigmoid)	60.5 ± 0.07
Conv2D(64, 2x2) → Flatten → Dense(128) → Dropout(0.4) →Dense(1, sigmoid)	59.5 ± 2.3
Conv2D(8, 2x2) → Conv2D(16, 2x2) → Flatten → Dropout(0.4) → Dense(1, sigmoid)	58.1 ± 2.7
Conv2D(16, 2x2) → Conv2D(32, 2x2) → Flatten → Dropout(0.4) → Dense(1, sigmoid)	60.6 ± 1.8
Conv2D(32, 2x2) → Conv2D(64, 2x2) → Flatten → Dropout(0.4) → Dense(1, sigmoid)	58.0 ± 2.1
Conv2D(64, 2x2) → Conv2D(128, 2x2) → Flatten → Dropout(0.4) → Dense(1, sigmoid)	62.2 ± 1.6
Conv2D(128, 2x2) → Conv2D(256, 2x2) → Flatten → Dropout(0.4) → Dense(1, sigmoid)	61.9 ± 1.1
Conv2D(64, 2x2) → BachNorm → Conv2D(128, 2x2) → BachNorm → Flatten → Dropout(0.4) → Dense(1, sigmoid)	63.8 ± 3.5
Conv2D(64, 2x2) → MaxPooling(2x2) → Conv2D(128, 2x2) → MaxPooling(2x2) → Flatten → Dropout(0.4) → Dense(1, sigmoid)	58.0 ± 1.7
Conv2D(64, 2x2) → BachNorm → MaxPooling(2x2) → Conv2D(128, 2x2) → BachNorm → MaxPooling(2x2) → Flatten → Dropout(0.4) → Dense(1, sigmoid)	58.1 ± 2.9
Conv2D(64, 3x3) → BachNorm → Conv2D(128, 3x3) → BachNorm → Flatten → Dropout(0.4) → Dense(1, sigmoid)	65.1 ± 3.6
Conv2D(64, 3x3) → BachNorm → Conv2D(128, 3x3) → BachNorm → Flatten → Dense(64) → Dropout(0.4) → Dense(1, sigmoid)	55.2 ± 9.6
Conv2D(64, 3x3) → BachNorm → Dropout(0.4) → Conv2D(128, 3x3) → BachNorm → Dropout(0.4) → Flatten → Dropout(0.4) → Dense(1, sigmoid)	61.2 ± 2.3
Conv2D(8, 2x2) → Conv2D(16, 2x2) → Conv2D(32, 2x2) → Flatten → Dropout(0.4) → Dense(1, sigmoid)	57.3 ± 5.4
Conv2D(16, 2x2) → Conv2D(32, 2x2) → Conv2D(64, 2x2) → Flatten → Dropout(0.4) → Dense(1, sigmoid)	59.1 ± 1.5
Conv2D(32, 2x2) → Conv2D(64, 2x2) → Conv2D(128, 2x2) → Flatten → Dropout(0.4) → Dense(1, sigmoid)	59.2 ± 2.0
Conv2D(64, 2x2) → Conv2D(128, 2x2) → Conv2D(256, 2x2) → Flatten → Dropout(0.4) → Dense(1, sigmoid)	63.6 ± 2.7
Conv2D(64, 2x2) → BachNorm → Conv2D(128, 2x2) → BachNorm → Conv2D(256, 2x2) → BachNorm → Flatten → Dropout(0.4) → Dense(1, sigmoid)	64.5 ± 2.3

Conv2D(64, 2x2) → MaxPooling(2x2) → Conv2D(128, 2x2) → MaxPooling(2x2) → Conv2D(256, 2x2) → MaxPooling(2x2) → Flatten → Dropout(0.4) → Dense(1, sigmoid)	63.4 ± 1.5
Conv2D(64, 2x2) → BachNorm → MaxPooling(2x2) → Conv2D(128, 2x2) → BachNorm → MaxPooling(2x2) → Conv2D(256, 2x2) → BachNorm → MaxPooling(2x2) → Flatten → Dropout(0.4) → Dense(1, sigmoid)	56.4 ± 4.0
Conv2D(64, 3x3) → BachNorm → Conv2D(128, 3x3) → BachNorm → Conv2D(256, 3x3) → BachNorm → Flatten → Dropout(0.4) → Dense(1, sigmoid)	**65.4 ± 1.4**
Conv2D(64, 3x3) → BachNorm → Conv2D(128, 3x3) → BachNorm → Conv2D(256, 3x3) → BachNorm → Flatten → Dense(64) → Dropout(0.4) → Dense(1, sigmoid)	48.9 ± 5.5
Conv2D(64, 3x3) → BachNorm → Dropout(0.4) → Conv2D(128, 3x3) → BachNorm → Dropout(0.4) → Conv2D(256, 3x3) → BachNorm → Dropout(0.4) → Flatten → Dropout(0.4) → Dense(1, sigmoid)	62.6 ± 3.1
Conv2D(64, 3x3) → BachNorm → Conv2D(128, 3x3) → BachNorm → Conv2D(256, 3x3) → BachNorm → Flatten → Dropout(0.2) → Dense(1, sigmoid)	65.2 ± 4.2
Conv2D(64, 3x3) → BachNorm → Conv2D(128, 3x3) → BachNorm → Conv2D(256, 3x3) → BachNorm → Flatten → Dropout(0.6) → Dense(1, sigmoid)	61.4 ± 3.6
Learning rate: 0.01; Batch size: 16	
Conv2D(64, 3x3) → BachNorm → Conv2D(128, 3x3) → BachNorm → Conv2D(256, 3x3) → BachNorm → Flatten → Dropout(0.4) → Dense(1, sigmoid)	60.6 ± 2.8
Learning rate: 0.0001; Batch size: 16	
Conv2D(64, 3x3) → BachNorm → Conv2D(128, 3x3) → BachNorm → Conv2D(256, 3x3) → BachNorm → Flatten → Dropout(0.4) → Dense(1, sigmoid)	60.7 ± 1.3
Learning rate: 0.001; Batch size: 8	
Conv2D(64, 3x3) → BachNorm → Conv2D(128, 3x3) → BachNorm → Conv2D(256, 3x3) → BachNorm → Flatten → Dropout(0.4) → Dense(1, sigmoid)	63.6 ± 2.6
Learning rate: 0.001; Batch size: 32	
Conv2D(64, 3x3) → BachNorm → Conv2D(128, 3x3) → BachNorm → Conv2D(256, 3x3) → BachNorm → Flatten → Dropout(0.4) → Dense(1, sigmoid)	64.1 ± 1.6

Appendix 2. Declaration of the use of artificial intelligence

Artificial intelligence was used only for English grammar checking and correction. The content was not generated by artificial intelligence.